The three-dimensional solar wind at solar activity minimum[1]

M. Neugebauer

Jet Propulsion Laboratory, California Institute of Technology, Pasadena

[1.] This paper is based on the Parker Lecture presented by the author at a meeting of the American Geophysical Union on December 9, 1997.

Abstract

In late 1997, the Ulysses spacecraft completed its first orbit around the Sun, observing the properties of the heliosphere at all latitudes between 80°S and 80°N. Because the mission occurred during a period of near-minimum solar activity, the configuration of the solar wind and interplanetary magnetic field were particularly simple, thus allowing confident comparisons between the properties of the polar corona observed by instruments on the Spartan and SOHO spacecraft and the resulting properties of the solar wind. Particular topics selected for review are the small amplitude variations (microstreams) in the speed of the fast polar solar wind, the large-scale three-dimensional configuration of the interplanetary magnetic field, the differences between transient solar wind events (coronal mass ejections) observed at intermediate and those seen at low latitudes, and the solar sources of the fast and slow solar wind.

Table of Contents

1. Introduction

In early 1998, the Ulysses spacecraft made history by completing a trip around the Sun in an orbit inclined to the solar equator by 80°. This first exploration of the Sun's polar regions led to many new insights into the three-dimensional structure of the heliosphere during a period of low solar activity. This review, however, covers only a few aspects of the Ulysses results, focusing on the solar wind plasma and the interplanetary magnetic field. Many rich and interesting topics, such as solar wind electrons, waves and turbulence, pickup ions of interstellar origin, energetic particles, and dust, are necessarily excluded.

Figure 1 [*McComas, et al.*, 1998] provides an overview of the latitudinal structure of the heliosphere during the first orbit of Ulysses. It is a polar plot of daily averages of solar-wind speed superimposed on three nested images of the Sun and its corona. The speed data have been color coded with red and blue to denote interplanetary magnetic fields pointing outward from and inward toward the Sun, respectively. The figure shows a dipolar structure, with an outward field in the north and an inward field in the south, and with fast wind over the poles and a rather narrow band of slow wind near the equator. This pattern results from the very simple structure of the Sun during this period of near-minimum solar activity.

In Figure 1 the image of the solar disk was obtained by the Extreme-Ultraviolet Imaging Telescope (EIT) on the SOHO spacecraft. The Sun's polar regions, which appear dark at those short wavelengths, are the relatively cool parts of the solar corona in which the magnetic field is open to space and the fast polar solar wind is accelerated. The part of the image just outside the solar disk was obtained by a coronagraph on Mauna Loa, Hawaii, operated by the High Altitude Observatory. It shows bright features called coronal streamers extending into space in the equatorial regions, with little emission over the poles. The outermost part of the image, from 1.5 to 6 solar radii (R_s), was obtained by the C2

coronagraph on SOHO; it shows the dense, bright part of the corona extending out into space in equatorial features called coronal streamers. Although the correspondence between the solar and coronal images and the speed of the solar wind is quite striking, one should not read too much into the details of the correlations because each solar image was obtained at one particular time while more than five years were required to build up the Ulysses data set. Nevertheless, the general correlation between fast, rather quiet wind over the polar coronal holes, and more variable, slow wind over the equatorial streamers was generally observed throughout this period.

2. Ulysses

Ulysses is a joint project of the US National Aeronautics and Space Administration (NASA) and the European Space Agency (ESA). ESA built the spacecraft, NASA launched it and tracks it, and operations are carried out by ESA personnel in NASA facilities. The instruments were provided by both US and European investigators. The spacecraft was launched in October, 1990, on a trajectory taking it from Earth to Jupiter, where, in February, 1992, it obtained a gravity assist into an eccentric, nearly polar heliocentric orbit. Figure 2 is a plot of latitude versus solar distance for that orbit. Each point in the figure represents a solar rotation (approximately 25.5 days) as seen from Ulysses.

Information on the spacecraft, trajectory, and instruments can be found in a special issue of *Astron. Astrophys. Supp., Ser. 92* , 207-440, 1992. There have been special issues of several journals that present results of different phases of the mission, including: *Geophys. Res. Lett., 19*, 1235-1314, 1992; *Science, 257*, 1503-1577, 1992; *J. Geophys. Res., 98*, 21111-21251, 1993; *Planet. Space Sci., 41*, 797-1108, 1993; *Space Sci Rev., 72*, 1-494, 1995; *Science, 268*, 1005-1036, 1995; *Geophys. Res. Lett., 22*, 3297-3432, 1995;

Astron. & Astrophys, 316, 279-563, 1996; and *J. Geophys. Res., 103*, 1889-2014, 1998. A book summarizing all the results of Ulysses' first orbit is in preparation.

3. The acceleration of the fast polar solar wind

Returning to Figure 1, note that the data acquired at aphelion are plotted on the right, while the perihelion data are on the left. On the right side, the highly variable speeds in the latitude range of 20-40°S resulted from the spacecraft alternating between high-speed and low-speed flows for part of each solar rotation, because during that particular phase of the solar cycle, the Sun's magnetic dipole had a greater latitudinal tilt than it had in the images shown in Figure 1. At the leading boundary of the high-speed streams, the fast wind overtakes the slower wind in its path, leading to a range of phenomena such as the generation of shocks and waves and the acceleration of energetic particles. The interesting physical processes observed in those corotating interaction regions are beyond the scope of this review, however. There are smaller variations and fewer interaction regions on the left side of Figure 1 because the tilt of the solar magnetic field had decreased to a value close to that in the figure and because near perihelion the spacecraft rapidly swept through the equatorial latitudes at a rate of ~22° per solar rotation.

The speed data are plotted in a different format in Figure 3. Here, the abscissa is the absolute value of heliographic latitude, and each point in the plot is the average speed observed over a solar rotation. The data from the southern and northern hemispheres are shown as dashed and solid lines, respectively. For latitudes equatorwards of ~±40°, the speed of the wind varied between high and low speeds, and the points in Figure 3 represent the average over all speeds encountered during a solar rotation. Poleward of ~±40°, however, no slow wind or systematic longitudinal variations were observed, but the average speed continued to increase with increasing latitude. The speed was systematically higher over the north polar region than over the south.

A long-standing question in space physics is the energy source for the acceleration of the solar wind [*Barnes*, 1992]. In *Parker's* [1958] original theory predicting the existence of the solar wind, the acceleration arose from classical thermal conduction from the hot (over 10^6 K) corona. Additional inputs of energy or momentum are believed to be required for the fast wind at low latitudes, but *Lallement et al.* [1986] interpreted observations of backscattered solar Lyman-α radiation in the polar regions to suggest that perhaps the polar solar wind flux was low enough that thermal conduction would suffice. Ulysses measurements have shown that although the solar wind flux in the polar regions is only about two-thirds of the average equatorial flux (i.e., $2x10^8$ $cm^{-2}s^{-1}$, rather than $3x10^8$ $cm^{-2}s^{-1}$), it is still great enough to require energy input over and above that from classical electron heat conduction [*Barnes et al.*, 1995].

Together with remote sensing of the solar corona with the SOHO spacecraft, the Ulysses measurements have yielded many clues about the acceleration mechanisms and have provided constraints that must be met by any model that is eventually accepted. Some of the most valuable new information comes from the SWICS instrument on Ulysses [*Gloeckler et al.*, 1992]. With that instrument it was possible to measure the charge states of many different ion species, (O, C, Si, Mg, and Fe). *Ko et al.* [1997] used the SWICS data to model the electron temperature profile in the corona as shown by the solid curve in Figure 4. The + signs in the figure show the temperature profile derived from the Spartan 201-01 coronagraph data [*Fisher and Guhathakurta*, 1995] based on the assumption of hydrostatic equilibrium. Note that the electron temperature derived from the Ulysses data peaks at ~$1.5x10^6$ K at a distance of ~1.4 R_s.

One of the remarkable and unexpected findings of the SWICS experiment is illustrated in Figure 5. It is a superposed epoch plot of the variation of solar wind speed (actually, the alpha-particle speed, which is sometimes slightly greater than the proton speed), ionization temperature (in 10^6 K) calculated from the distribution of charge states of oxygen ions, and the ratio of the flux of Mg to O ions, all observed as Ulysses moved back and forth

between high and low speed streams during each solar rotation in late 1992 and early 1993. The figure shows there was an anti-correlation between solar wind speed and ionization temperature; i.e., the fastest wind came from the coolest part of the corona. It also shows that there was a direct correlation between ionization temperature and the ratio of abundances of easily ionized magnesium to oxygen which has a higher first-ionization potential. These correlations show a connection between the pickup of solar material as it first becomes ionized in the chromosphere, the temperature higher up in the solar atmosphere in the corona where ionization equilibium is reached, and the acceleration which occurs even higher in the corona, indicating that all three regions and processes must be physically linked. These results force us to think of the whole chain of events as interrelated processes; it is no longer possible to start theories of the acceleration of the solar wind with a boundary condition of a hot corona with a given chemical composition which has been heated by some independent and irrelevant process.

Recent results from the Ultra-Violet Coronagraph Spectrograph (UVCS) on the SOHO spacecraft provide more information about how the corona is heated and the solar wind is thereby accelerated. UVCS measures the intensities and profiles of the hydrogen Lyman-α line and two lines of the O^{5+} ion in the corona from 1.5 to 5 R_s. When the data are interpreted in terms of the "thermal" motions in the solar radial and latitudinal directions as well as the outflow velocities and then combined in an empirical model of the coronal hole, the following results are found [*Kohl et al.,* 1997; *Cranmer et al.,* 1998]:

(1) The "thermal" (random motion) velocities of the O^{5+} ions are much greater perpendicular to the magnetic field than parallel to it (the field was assumed to be in the radial direction).

(2) The perpendicular component of the "thermal" velocity is much greater for O^{5+} ions than for protons.

(3) The outflow speed of O^{5+} ions is greater than the outflow speed of protons, which in turn is greater than that expected for electrons.

These observations are not only inconsistent with thermodynamic equilibrium but are also inconsistent with any common motions of the two ion species; i.e., the "thermal" speeds cannot be due to transverse waves (such as Alfvén waves) or turbulent motions. *Cranmer et al.* [1998] suggest that the observations can be accounted for by ion-cyclotron waves. This is consistent with a scenario proposed by *McKenzie et al.* [1995] wherein the heavier ions are preferentially heated by resonant dissipation of high-frequency ion-cyclotron waves generated by microflares at supergranule boundaries on the solar surface. But we still do not yet have an end-to-end theory or numerical model that predicts how microflares, or the plasma jets proposed by *Feldman et al.* [,1996] to account for the kinetic properties of alpha particles in the solar wind, generate the spectrum of waves required to match the SOHO UVCS observations or the observed properties of solar wind ions at 1 AU.

4. Microstreams in the polar solar wind

Although it is apparent from Figure 1 that the speed of the high-latitude solar wind was remarkably steady in comparison to the speeds observed in equatorial regions, the jitter in the plot indicates that the polar solar wind was not without structure. Figure 6 provides power spectra of the fluctuations in the three components of the proton velocity vector in the high-speed wind from the south polar coronal hole. The component axes are $\mathbf{R}$ = radially outward from the Sun, $\mathbf{T}$ = tangential = $\Omega \times \mathbf{R}$, and $\mathbf{N}$ = normal = $\mathbf{R} \times \mathbf{T}$, where Ω is parallel to the solar rotation vector. For periods shorter than about half a day, there is a similar amount of power in all three axes, whereas at longer periods the power in the radial component exceeds that in the two transverse components. The transverse fluctuations are due largely to a high flux of outward propagating Alfvén waves. The radial component, however, reveals a significant structure in the high speed wind.

A sample of these speed variations, together with information on simultaneous pressure variations, is shown in Figure 7. The top trace of this figure shows hourly average speed measured by Ulysses between April 1 and April 24, 1994, when Ulysses was at a solar latitude of ~60° South. At this time resolution, it is seen that the speed varies between ~700 and 800 km/s, with the principal peaks or valleys separated by ~3 days. The middle trace in Figure 7 shows the plasma pressure (nkT) in the reference frame of the solar wind, while the bottom trace shows the magnetic pressure ($B^2/8\pi$).

The most prominent structure in Figure 7 was associated with a coronal mass ejection (CME). CMEs are discussed further in Section 6; here it is only noted that there were large enhancements of both the plasma and magnetic pressures following a forward shock (FS) and preceding a reverse shock (RS) caused by the interplanetary expansion of the CME.

The plasma pressure enhancement marked as "pressure balance" in Figure 7 is accompanied by a decrease in the magnetic pressure such that the total pressure remains constant. *Thieme et al.* [1988; 1990] reported the observation of similar pressure-balance structures in the near-equatorial high-speed wind by the Helios spacecraft and postulated they were related to modulation of the solar wind by the solar supergranulation structure related to the patterns of convection in the outer layers of the Sun. *McComas et al.* [1995] initially suggested that the pressure-balance structures observed by Ulysses might be related to polar plumes, which are bright, ray-like structures seen in images of the polar solar corona. A more extensive study [*McComas et al.*, 1996], however, led to the conclusion that the pressure-balance structures are probably not the interplanetary signatures of polar plumes because they do not have any characteristically different plasma or field properties from the rest of the solar wind.

If pressure-balance structures are not the interplanetary manifestation of polar plumes, the principal plume candidates are the speed variations evident in Figure 7. These structures, which have been called "microstreams" by *Neugebauer et al.* [1995], do exhibit several distinctive properties, some of which are summarized in Figure 8. That figure is a

superposed epoch analysis of 6-hour averages centered on 29 well-resolved peaks and 17 well-defined dips in the solar wind speed during the seven solar rotations when Ulysses was poleward of 60°S in 1994. The top panel shows the radial component of the proton velocity (very nearly equal to the proton speed) which, on the average, was ~50 km/s higher at the peaks than at the dips. The second panel shows the normalized proton flux ($n_p v_p r^2$), which was greatest on the leading edges of the peaks and lowest just ahead of the dips, as expected by compression and rarefaction waves ahead of and behind the fast streams, respectively. Note that the flux was the same at the top of the peaks as at the bottom of the dips. The proton temperature, normalized by an $r^{-0.51}$ fit to all the data acquired in the flow from the southern polar coronal hole, showed that the fast plasma was hotter than the slow plasma, after the effects of compression and rarefaction are accounted for. Finally, the bottom panel shows that the fast plasma in the peaks had a greater helium abundance than did the slow plasma in the dips. If either the fast, hot, helium rich wind in the peaks or the slower, cooler, relatively helium-poor wind is related to the polar plumes, it is not yet known which is the plume material and which originates in the interplume regions of the corona.

If the microstreams are the interplanetary signatures of stationary structres with uniform size, then the time required for a structure to corotate past Uysses would increase with latitude as $1/\cos\lambda$. No latitudinal dependence of microstream width was detected, however, which leads to the conclusion that the solar counterparts of the microstreams probably have a temporal component, with a lifetime no longer than two or three days. Early observations suggested that individual plumes have lifetimes of several hours to several days, with an average of ~15 hours. A recent campaign to observe polar plumes with 6 separate instruments on SOHO revealed rapid (10-minutes to hours) changes in detailed substructures and in overall birightness, but that the large-scale location and shape remained steady over the course of the 16-hour observation period and that the brightest plumes could be seen on the previous and following days [*DeForest et al.*, 1997].

Although plumes remain a possible source of microstreams, there are other possibilities. Even though the microstreams are most readily recognizable in the high-latitude solar wind near solar-activity minimum, they are almost certainly not limited to high latitudes. In some respects they resemble in-ecliptic features which *Burlaga* [1975] has related to the ubiquitous irregular variations of the solar wind which exhibit a fractal structure. Alternatively, the low-frequency peaks in the radial-component power spectrum shown in Figure 6 closely agree with some of the peaks of fluctuations in energetic particle fluxes which *Thomson et al.* [1995] have suggested are caused by gravity-wave excitations (g-modes) of the Sun. Finally, *Roberts and Goldstein* [1998] have suggested that the spectral peak near 3.3 days, which corresponds to a typical time between consecutive peak speeds of the microstreams, may simply be the tenth harmonic of the ~34-day rotation period of magnetic features at latitudes near 70° latitude.

5. The interplanetary magnetic field

The polar plot of the solar wind speed shown in Figure 1 is color coded according to the direction of the interplanetary magnetic field (IMF), with red denoting positive field directions, pointing out of the Sun, and blue denoting negative, inward fields. These directions are consistent with the current magnetic polarity of the Sun, which has outward fields in its north polar cap and inward fields in the south. Figure 9 shows a different representation, with the daily average radial component of the IMF, scaled by the square of the distance from the Sun, plotted versus time for the fast latitude scan from 80°S to 80°N in 1994-5; the heliographic latitude of Ulysses is shown at the top of the figure. As in Figure 1, it is seen that the field was consistently negative for latitudes below 35°S and positive for latitudes above 20°N, with mixed polarities at low latitudes [*Smith et al.*, 1997].

For all solar distances for which the direction of the solar wind velocity vector has been measured (i.e., distances >0.3 AU), the flow is nearly radial with deflections no more than a few degrees resulting from waves and the interactions of fast and slow solar wind streams. If the flow were radial all the way out from the solar surface, the field at high latitudes would be stronger than the equatorial field because one of the properties of a dipole field is that its strength increases poleward. Figure 9 shows, however, that the strength of the normalized radial component of the IMF was ~3 nT-AU^2, independent of latitude. The implication of this observation is that there is strong non-radial flow in the lower corona where the magnetic pressure is so much greater than the plasma pressure that the strong polar fields force the plasma equatorward to equalize the pressure. This process has been studied theoretically by *Suess* [1979] and *Suess and Smith* [1996].

What about the direction of the IMF? The simplest model, to which data are often compared, is that of the Parker spiral [*Parker,* 1958], given by:

$$B_R/B_o = (R_s/R)^2 \tag{1}$$

$$B_T/B_o = \Omega R_s^{\,2} \cos\lambda/vR \tag{2}$$

$$B_N/B_o = 0 \tag{3}$$

where B_R is the radial component of the magnetic field, B_T is the tangential component defined by the cross-product of the radius vector with the solar rotation vector Ω, while the normal component B_N completes a right-handed system, R is distance from the Sun, R_s is the solar radius, v is the solar wind speed, and λ is heliographic latitude. B_o is the field at the surface of the Sun, which is assumed to be radial. The radial component B_R decreases as R^{-2} to conserve magnetic flux ($\nabla \bullet B = 0$), while the rotation of the Sun drags around the footpoints of the field lines, which remain anchored in the Sun, to form the spiral pattern. From (1) to (3), one sees that the direction of the IMF is expected to vary along the Ulysses trajectory in response to changes in R, λ, and v. This nominal, Parker-spiral variation of the radial component B_R normalized by the field magnitude B is shown as a function of latitude by the heavy line in Figure 10. The calculation was based on solar rotation

averages of hourly averages of the field components, the field magnitude, and the speed and on the (sidereal) rotation rate of the magnetic field at the solar surface given by [*Snodgrass* , 1983]:

$$\Omega = 3.101 - 0.464 \sin^2\lambda - 0.328 \sin^4\lambda \ \mu\text{rad/s} \quad (4)$$

Starting near the center of the diagram, one sees the Parker spiral becoming more tangential and therefore less radial as the spacecraft moved away from the Sun toward Jupiter near the equatorial plane. Then after the Jupiter flyby, the spacecraft moved simultaneously inward and southward until reaching 80°S. The fast-latitude scan took the spacecraft inward to perihelion at 1.3 AU and then slightly outward again to 80°N. The fine-scale bumps in the curve are caused by variations in the solar wind speed encountered at low latitudes.

The dashed line in Figure 10 shows the observed field direction computed from hourly averages of B_R and B. The figure shows very little dependence on latitude and smaller-than-predicted dependence on distance from the Sun. In fact, the fields during the fast-latitude scan were only slightly more radial, and the fields during the aphelion phase of the trajectory were only slightly less radial than the value of 0.5 expected for random variations in direction, indicated by the thin solid line. (Note: Because of the presence of waves, a slightly different result would have been obtained if $\langle B_R \rangle$ had been normalized by $(\langle B_R \rangle^2 + \langle B_T \rangle^2 + \langle B_N \rangle^2)^{1/2}$ instead of by $\langle B \rangle$, where $\langle\ \rangle$ denotes the hourly averages used in the construction of Figure 10. Both the observational values (dashed line) and the value expected from random fluctuations (thin line) would move up by a factor of $2/\sqrt{3} = 1.155$, but the qualitative result would remain the same.)

Using a different method of analysis, *Forsyth et al.* [1996] compared the measured spiral angle ($\phi_B = \tan^{-1} B_T/B_R$) to the angle ϕ_P expected for the Parker spiral; their high-latitude results are shown in Figure 11 as histograms of hourly-averaged field directions divided into 10°-bins of $\phi_B - \phi_P$. While the most probable direction of the field in the southern hemisphere was 24° more tightly wound than the Parker spiral, the field in the northern hemisphere agreed well with the Parker model.

Can we reconcile the apparent disagreement between Figures 10 and 11 and is there a better model of the three-dimensional IMF than the Parker spiral? Two factors are important: waves and an initial configuration near the Sun that is more complex than that assumed by Parker. Each of these is discussed below, starting with waves.

As Ulysses passed to higher latitudes and the solar wind speed became appreciably steadier than it had been at lower latitudes (see Figure 1), the hourly variances of each of the components of the magnetic field and the velocity steadily increased. The fluctuations in $\boldsymbol{B}$ and $\boldsymbol{v}$ had all the properties expected of Alfvén waves propagating away from the Sun: the transverse components of $\boldsymbol{B}$ and $\boldsymbol{v}$ were highly correlated over a broad frequency range corresponding to periods <1 to >10 hours while the magnitudes B and v were nearly constant [*Smith et al.*, 1995]. Figure 12 shows solar-rotation averages of the hourly correlation between the normal components B_N and v_N over the course of the Ulysses mission. For pure outwardly propagating Alfvén waves, this correlation would be +1 in the southern hemisphere and -1 in the north. Following along the Ulysses trajectory, the figure shows very little correlation out to Jupiter, at distances >4 AU, or at the perihelion equatorial crossing, but strong correlations in the solar wind from the polar coronal holes.

What generates these waves? One idea is that they are unabsorbed remnants of the wave field that heats the corona and accelerates the solar wind to high speeds in coronal holes. As discussed above in Section 3, however, recent observations suggest that higher-frequency ion-acoustic waves may play a more important role. Another source of transverse waves is summarized by the cartoon in Figure 13 from a paper by *Jokipii and Kota* [1989]. Long before there were any high-latitude data from Ulysses, they suggested that the motions of the footpoints of interplanetary magnetic field lines caused by convection in the outer layers of the Sun would generate a transverse component of the high-latitude IMF. These disturbances would travel out along the field lines as Alfvén waves. But in addition to the large perturbations due to waves, several modifications to the underlying Parker field may be necessary. The Parker spiral is based on the assumption

that the field at the Sun is purely radial, whereas the footpoint motions suggested by Jokipii and Kota and illustrated in Figure 13 lead to transverse fields. If there are substantial horizontal motions of the field footpoints, as shown in the figure, then the magnitude of the polar IMF would decrease as $1/R$, as opposed to the $1/R^2$ fall off of the mainly radial polar field in the Parker model.

Another modification was proposed by *Smith and Bieber* [1991] from their study of solar cycle variations of the IMF in the ecliptic plane. They suggested that there was a transverse component of the field at the Sun arising from the differential rotation of the solar magnetic field as well as from the latitudinal transport of field lines discussed above in connection with the latitudinal independence of the radial component of the IMF.

The most recent model of the IMF is by *Fisk* [1996]. His model takes into account (a) the angular offset or tilt between the Sun's rotation axis and the axis of its magnetic dipole, (b) the latitudinal flow, discussed above, from the regions of high magnetic pressure near the magnetic pole to lower magnetic latitudes, (c) the differential or latitude dependent rotation of the solar magnetic field as given by equation (4), and (d) the rigid, latitude-independent rotation of the boundaries of the coronal holes from which the high-speed wind comes. The general picture is that closed magnetic loops open as they differentially rotate into a coronal hole and then reconnect to close again when they reach the other boundary. The result is a complicated geometry in which an interplanetary field line may be observed at a latitude more than 40° away from the latitude at which its footpoint is tied to the Sun. Figure 14 contrasts the complex traces of field lines emanating at a solar latitude of 70°S for the Fisk model with the simple field lines corresponding to the basic Parker model.

A phenomenon that is closely tied to the 3-dimensional structure of the IMF, and which may serve as a discriminator between the several different models of the IMF, is the modulation of galactic cosmic rays. These energetic particles originating outside the solar system must work their way through the outwardly moving IMF to reach the inner solar

system. The lowest energy cosmic rays are affected the most, and their flux is generally lowest when solar activity is a maximum. The entry of cosmic rays into the inner heliosphere is believed to be controlled by diffusion, outward convection, adiabatic cooling, and electromagnetic drifts in the IMF [*Jokipii et al.,* 1977; 1986]. Before Ulysses, it had been expected that for the present polarity of the solar magnetic field, the drift motions would be such that positively-charged cosmic rays would have easy access over the solar poles, leading to a large increase in their flux as Ulysses climbed to higher latitudes. Only a very modest increase was observed, however [e.g., *Simpson et al.,* 1995].

One effect working against a large increase in low energy cosmic rays at high latitudes is the stronger-than-Parker polar fields caused by the transverse footpoint motions suggested by *Jokipii and Kota* [1989]. The large amplitude Alfvén waves also contribute. Alfvén waves with periods of 1 to 10 hours have wavelengths of ~0.02 to 0.2 AU and resonate with cosmic rays having energies of ~10 MeV/nucleon to 1 GeV/nucleon [*Smith et al.,* 1995]. Figure 14 [*Heber et al.,* 1996] compares the observed latitude variations of the fluxes of cosmic-ray protons in three different energy ranges during the Ulysses fast latitude scan with predictions of the Parker spiral model and the *Smith and Bieber* [1991] model. Waves are accounted for in these calculations by adjustment of the diffusion coefficients. For all three energy ranges, the Smith and Bieber model gives an appreciably closer fit to the observations than does the Parker-spiral model, but further modification is required to fit the lowest energy data. No one has yet calculated the cosmic-ray modulation expected on the basis of Fisk's model of the IMF.

6. Coronal mass ejections in the polar solar wind

Up to this point, this review has considered the quasi-stationary solar wind whose patterns and properties do not change very much over periods of weeks or months.

Another component of the solar wind arises from transient solar events, the most important of which for heliospheric physics is the coronal mass ejection (CME). Even though solar activity was in a fairly low state during the first polar orbit of Ulysses, and even though CMEs tend to occur close to or within the streamer belt which straddles the magnetic equator [*Hundhausen*, 1993], Ulysses did observe a few CMEs in the fast polar solar wind at intermediate, but not at the very highest latitudes. When seen in the solar wind, some properties of the CMEs at higher latitudes are quite different from the low-latitude CMEs which have been studied for several decades. The major differences are summarized in Table 1.

First, the CME material observed in the polar solar wind usually has a greater speed than it has in the ecliptic. This feature is summarized in Figure 16. The top panel shows the distribution of the speeds of CMEs observed by the coronagraph on the Solar Maximum Mission (SMM) as the structures moved out from the Sun through the corona; most of the CMEs observed in this way had speeds <500 km/s. The bottom panel shows the distribution of speeds of CME material observed near Earth by the ISEE-3 spacecraft together with the speed distribution of all the solar wind observed by ISEE 3. Each of these three curves peaks at very roughly the same speed (350 ± 100 km/s). What was surprising was that every one of the six CMEs detected by Ulysses when it was in the polar solar wind, at latitudes between 31°S and 61°S, had speeds >650 km/s. This is much faster than the speed at which most CMEs leave the Sun and indicates that processes must be at work to accelerate the transient plasma up to the speed of the ambient, quasi-stationary wind with which it interacts. In retrospect, those same processes are probably responsible for the close similarity between the two distributions in the bottom panel of Figure 16, with the CME speeds, on average, being only slightly greater than the average speeds observed by ISEE 3. The fastest CMEs are slowed down while the slowest ones are accelerated during their interplanetary transit. What is the process that brings the transient wind to a speed approximating that of the ambient wind? Several suggestions have been made

[*Gosling, et al.*, 1994a; *Cargill et al.*, 1996], but to my mind the most convincing argument is based on the dynamic interaction of the CME plasma with the solar wind ahead of and behind it, as modeled in one dimension by *Gosling and Riley* [1996] and *Gosling et al.* [1998]. The basic idea is that if a plug of slow plasma (from the CME) is inserted into a fast-moving wind, it will be pushed on by the fast plasma behind it and will also be accelerated by the pressure gradient at its leading edge into the rarefaction caused by the plasma ahead running away from it. This model does not, however, address the question of how the slow CME plasma was inserted into the fast wind in the first place.

Near the ecliptic plane, when the CME plasma from energetic solar events moves faster than the ambient wind, it is preceded by a compressional or bow wave which sometimes steepens into a shock. A surprising feature of many of the CMEs in the polar solar wind was the existence of compressional waves or shocks both ahead of and behind the CME plasma. Figure 17 shows a CME event that was observed both near Earth by IMP 8 (data on the left) and at high latitude by Ulysses (data on the right); this CME has been discussed in detail by *Goslling et al.* [1995b]. Near Earth, only a forward shock (labeled "F. shock") was observed, whereas at Ulysses, there was a forward shock moving into the ambient wind ahead of the CME as well as a reverse (R.) shock traveling back upstream toward the Sun, in the reference frame of the solar wind. At Ulysses, the speed of the CME plasma (shown in the third panel) was approximately the same as the sped of the ambient wind ahead of the forward shock and sunward of the reverse shock, so it was not the speed difference that generated the shocks. *Gosling et al.* [1994b, 1998] argue that it is the strong expansion of the CME material, from an initial pressure much higher than that of the ambient plasma, which generates a shock wave traveling outward into the ambient plasma in all directions.

The next row in Table 1 refers to one of the methods by which CME plasma can be identified in the solar wind. For the quasi-stationary wind, the magnetic fields are open, meaning that one "end" of the field line is at the Sun while the other end has been carried

away by the solar wind (Although an open field line apparently violates Maxwell's equation $\nabla \bullet \mathbf{B} = 0$, one can wave one's arms and declare that the Sun's open field lines close at infinity, or the very outer heliosphere.). Because the coronal electron temperature is high, measurements of interplanetary electrons revea anti-sunward high-energy tails to the electron distributions, which are equivalent to a heat flux away from the Sun. A CME is thought to involve the expulsion of plasma and field lines that had been closed loops before the event. The result is the extension of magnetic loops into space, with both ends of the field lines still attached to the Sun until a magnetic rearrangement or reconnection takes place. Figure 18 illustrates this concept. When both ends or footpoints of a magnetic field line go through the hot corona, there is a high-energy electron tail from each end of the loop to yield what is called bi-directional electron streaming. This feature is a useful identifier of CME plasma at both low and high latitudes. The intervals labeled "CME" in Figure 17 were identified in that way. Although bidirectional electron streaming is observed in CMEs at both low and intermediate latitudes, it is not a necessary condition for the identification of CME plasma in the solar wind because if one of the legs of the magnetic loop reconnects to the ambient IMF, the bidirectional streaming ceases.

In about one third of the CMEs identified in the low-latitude solar wind, the magnetic field appears to be twisted into a flux rope [*Gosling,* 1990], as sketched in Figure 18. Only one of the six CMEs observed in the polar solar wind by Ulysses exhibited such a flux-rope geometry, but more examples are required to determine whether or not there is a systematic dependence of the magnetic topology on latitude.

Another signature of CMEs at low latitudes is a change in the charge-state distribution of heavy ions. In some events, the heavy ions are more highly ionized than they are in the quasi-stationary solar wind, in keeping with the observation that coronal plasma on closed magnetic loops is hotter than that on open field lines. In some events, the low latitude CMEs show a mixture of charge states, with both highly charged (hot) distributions and very low charge states, such as He^{+}. The cold component may originate

in low-lying magnetic structures, such as solar prominences, which pass through the hot corona without coming to thermodynamic equilibrium. As Ulysses moved to higher latitudes, the distribution of charge states in CME plasma shifted to lower values, as shown in Figure 19 [*Galvin,* 1997].

The final latitude-related difference in CME plasma listed in Table 1 is the helium (alpha-particle) abundance. Near the ecliptic, CMEs often contain plasma highly enriched in alphas relative to protons, sometimes reaching density ratios n_α/n_p of ~0.5, compared to an average value of ~0.05. The helium enhancements are patchy, sometimes present, sometimes not. No large helium enrichments were observed, however, in any of the six intermediate-latitude events detected by Ulysses [*Barraclough et al.,* 1996]. For the CME shown in Figure 17, n_α/n_p reached ~0.20 near Earth, but did not exceed 0.08 at Ulysses.

None of the differences between the low- and the intermediate-latitude CMEs had been predicted. The first two differences listed in Table 1 can be explained in terms of the interaction of the CMEs with their surroundings. The reasons for the last two, or perhaps the last three, differences are not yet clear. The lack of helium enhancements and of high-ionization states might be interpreted as evidence that the CMEs in the polar solar wind originated on field lines that were already open, but the observation of a flux-rope geometry in one of the intermediate-latitude events would argue against such an interpretation.

7. Solar sources of the solar wind

In the discussions in the previous sections, especially in Section 5 dealing with the invariance of the normalized radial component of the magnetic field with latitude, it was tacitly assumed that the quasi-stationary (i.e., the non-CME) high-speed solar wind observed by Ulysses at latitudes poleward of 20 or 30° all originated in the polar coronal holes. This assumption requires strong non-radial flow close to the Sun from the polar regions to lower latitudes. *Gosling et al.* [1995a] estimated that the Sun-centered solid-

angle occupied by the fast polar solar wind increased by a factor of ~4.8 between the Sun and Ulysses. That assumption has recently been challenged by several papers in which near-solar data are interpreted as suggesting that the fast wind flows radially away from the Sun with no latitudinal expansion [*Woo and Habbal,* 1997; *Habbal et al.,* 1997]. The suggestion of radial flow of the fast wind from regions of the solar surface outside the polar coronal holes was based on interpretation of Figure 20. The figure shows a highly processed image of the inner corona from the Mauna Loa coronagraph together with red lines which are a polar plot of the total electron content between the Earth and Ulysses as a function of the latitude of the points of closest approach to the Sun of the Earth-Ulysses radio ray path. It should be noted that although the radio data are plotted so they overlap the coronagraph image inside 2 R_s, the data were actually acquired at solar distances > 20 R_s. I believe that the evidence for latitudinal expansion of the fast solar wind from the polar coronal holes outweighs that for the radial flow hypothesis[*Woo and Habbal,* 1997; *Habbal et al.,* 1997] for a number of reasons:

(1) Extrapolations of coronagraph images of solar features such as rays and streamers back to the Sun converge on the polar regions rather than on the center of the solar disk. An example is shown in Figure 21, where I have overlaid dashed lines on a figure from *Habbal et al.* [1997].

(2) There is a strong, well documented correlation between equatorial extensions of polar coronal holes and high-speed wind seen in the ecliptic [*Nolte et al.,* 1976]. There is also a good correlation between the size of the coronal-hole extension within 10° of the ecliptic and the solar wind speed [*Nolte et al.,* 1976].

(3) The magnetic polarity of the high-speed wind matches that of the polar coronal hole in the hemisphere in which the high-speed wind is observed. If the fast wind flows out radially from magnetically open regions at intermediate-latitudes, those regions must have the magnetic polarity of the nearby polar coronal hole.

(4) Similarly, if the fast wind flows out radially from magnetically open regions at intermediate latitudes, the temperature profile in the corona above those regions must be similar to that above the polar coronal holes in order to explain the low ionization temperature of all the heavy ions in the high-speed solar wind. There is currently no evidence for low coronal temperatures other than in coronal holes.

(5) Several different models (both magnetohydrodynamic and potential-field models) of the interplanetary magnetic field using the magnetic field observed at the solar surface as a boundary condition indicate that the fast wind emanates from the polar coronal holes [*Neugebauer et al.,* 1998]. Those models would not be valid, however, if the intermediate-latitude fast wind came from regions that were magnetically open to space for only a short time compared to the synoptic (27-day) magnetic maps used as input to the models.

(6) Empirically, there is a good correlation between the observed solar wind speed and the factor by which the magnetic field expands between the Sun and interplanetary space [e.g., *Wang et al.,* 1997]. Such a correlation has some basis in the theory of the acceleration of the solar wind [*Wang and Sheeley,* 1991]. As with the previous issue, however, the expansion factors are calculated from synoptic data of the solar magnetic field and does not have any contribution from any transiently open or small-scale fields.

(7) As discussed in Section 5, the solar surface shows significant differential rotation, with features at high latitudes rotating more slowly than near-equatorial features (see Eq. 4). *Roberts and Goldstein* [1998] have found two fundamental periodicity's in the solar wind observed by Ulysses near 25° S latitude: a 26-day variation characteristic of equatorial regions and of the boundaries of coronal holes, which do not exhibit differential rotation, and a 34-day variation characteristic of other surface features at latitudes near ±70°. At higher latitudes, where the spacecraft was constantly embedded in high speed flow, only the 34-day periodicity and its harmonics were detected. This result is

interpreted as providing support for the solar wind observed near 25° latitude originating at a latitude near 70°.

(8) Figure 22 shows the distribution of the intensity of Lyman-α radiation observed in the solar corona by the UVCS instrument on SOHO; the abscissa is the polar angle (complement of latitude) and the circles are the observations. Two model curves are shown, one for purely radial flow, consistent with the suggestion by *Woo and Habbal* [1997], and the other for a model in which the polar magnetic fields expand down to near-equatorial latitudes. The non-radial model clearly provides the better fit to the data.

In summary, I believe that the apparent radial alignment of the several features noted by *Woo and Habbal* [1997] is not sufficient evidence for radial flow of the high-speed solar wind.

In the quasi-stationary state, where does the slow solar wind come from? There are several candidate locations: the boundary regions of the polar coronal holes, bright coronal streamers like those seen in Figures 1 and 21, and small low-latitude coronal holes. In many models, these first two sources of the low-speed wind are the same; plasma is thought to flow latitudinally from the coronal hole boundaries, around the closed field lines at the base of a streamer, and then outward along the streamer "stalk". Recent radio observations [*Woo and Martin,* 1997] are consistent with such a view. But when MHD or potential field models are used to trace back the origin or footpoints of interplanetary field lines carried by the slow solar wind, some of the footpoints trace back to the regions just outside the polar coronal holes while others are found to originate in isolated small coronal holes at low latitudes [*Neugebauer et al,,* 1998]. I currently believe that both types of sources contribute to the low speed solar wind, but it is a topic worthy of further analysis.

Acknowledgments. This research was performed at the Jet Propulsion Laboratory under a contract between the California Institue of Technology and the Naitional Aeronautics and Space Administration.

References

Barnes, A., Acceleration of the solar wind, *Rev. Geophys., 30*, 43-55, 1992.

Barnes, A., P. R. Gazis and J. L. Phillips, Constraints on solar wind acceleration mechanisms from Ulysses plasma observations: The first polar pass, *Geophys. Res. Lett., 22*, 3309-3311, 1995.

Barraclough, B. L., W. C. Feldman, J. T. Gosling, D. J. McComas, J. L. Phillips and B. E. Goldstein, He abundance variations in the solar wind: Observations from Ulysses, in *Solar Wind Eight, AIP Conference Proceeding 382,* edited by D. Winterhalter, J. T. Gosling, S. R. Habbal, W. S. Kurth and M. Neugebauer, pp 277-280, Amer. Inst. Phys., Woodbury, NY, 1996.

Burlaga, L. F., Interplanetary streams and their interaction with the Earth, *Space Sci. Rev., 17*, 327, 1975.

Cargill, P. J., J. Chen, D. S. Spicer, and S. T. Zalesak, Magnetohydrodynamic simulations of the motion of magnetic flux tubes through a magnetized plasma, *J. Geophys. Res., 101*, 4855, 1996.

Cranmer, S. R., et al., An empirical model of a polar coronal hole at solar minimum, *Astrophys. J.,* Submitted, 1998.

DeForest, C. E., Polar plume anatomy: Results of a coordinated observation, *Solar Phys., 175*, 393, 1997.

Feldman, W. C., S. R. Habbal, G. Hoogeveen and Y.-M. Wang, Experimental constraints on pulsed and steady state models of the solar wind near the Sun, *J. Geophys. Res., 102*, 26,905, 1997.

Fisher, R., and M. Guhathakurta, Physical properties of polar coronal rays and holes as observed with SPARTAN 201-01 coronagraph, *Astrophys. J., 447*, L139, 1995.

Fisk, L. A., Motion of the footpoints of heliospheric magnetic field lines at the Sun: Implications for recurrent energetic particle events at high heliographic latitudes, *J. Geophys. Res., 101*, 15,547-15,553, 1996.

Forsyth, R. J., A. Balogh, T. S. Horbury, G. Erdös, E. J. Smith and M. E. Burton, The heliospheric magnetic field at solar minimum: Ulysses observations from pole to pole, *Astron. Astrophys., 316*, 287-295, 1996.

Galvin, A. B., Minor ion composition in CME-related solar wind, in *Coronal Mass Ejections, Geophsical Monograph 99,* edited by N. Crooker, J. A. Joselyn and J. Feynman, pp 147-156, Amer. Geophys. Un., Washington, DC, 1997.

Geiss, J., G. Gloeckler, and R. von Steiger, Origin of the solar wind from composition data, *Space Sci. Rev. 72*, 49, 1995.

Gloeckler, G. L., et al., The solar wind ion composition spectrometer, *Astron. Astrophys. Suppl., 92*, 267, 1992.

Gosling, J. T., Coronal mass ejections and magnetic flux ropes in interplanetary space, in *Physics of Magnetic Flux Ropes,* edited by C. T. Russell, pp 343, American Geophysical Union, Washington, DC, 1990.

Gosling, J. T. and P. Riley, The acceleration of slow coronal mass ejections in the high-speed solar wind, *Geophys. Res. Lett., 23*, 2867, 1996.

Gosling, J. T., Corotating and transient solar wind flows in three dimensions, *Ann. Rev. Astron. Astrophys., 34*, 35, 1996.

Gosling, J. T., S. J. Bame, D. J. McComas, J. L. Phillips, B. E. Goldstein and M. Neugebauer, The speeds of coronal mass ejections in the solar wind at mid heliographic latitudes: Ulysses, *Geophys. Res. Lett., 21*, 1109, 1994a.

Gosling, J. T., D. J. McComas, J. E. Phillips, L. A. Weiss, V. J. Pizzo, B. E. Goldstein and R. J. Forsyth, A new class of forward-reverse shock pairs in the solar wind, *Geophys. Res. Lett., 21*, 2271, 1994b.

Gosling, J. T., S. J. Bame, W. C. Feldman, D. J. McComas, J. L. Phillips, B. Goldstein, M. Neugebauer, J. Burkepile, A. J. Hundhausen and L. Acton, The band of solar wind variability at low heliographic latitudes near solar activity minimum: Plasma results from the Ulysses rapid latitude scan, *Geophys. Res. Lett., 22*, 3329-3332, 1995a.

Gosling, J. T., D. J. McComas, J. L. Phillips, V. J. Pizzo, B. E. Goldstein, R. J. Forsyth and R. P. Lepping, A CME-driven solar wind disturbance observed at both low and high heliographic latitudes, *Geophys. Res. Lett., 22*, 1753, 1995b.

Gosling, J. T., P. Riley, D. J. McComas and V. J. Pizzo, Overexpanding coronal mass ejections at high heliographic latitudes: Observations and simulations, *J. Geophys. Res., 103*, 1941, 1998.

Habbal, S. R., R. Woo, S. Fineschi, R. O'Neal, J. Kohl, G. Noci and C. Korendyke, Origins of the slow and the ubiquitous fast solar wind, *Astrophys. J., 489*, L103, 1997.

Heber, B., W. Dröge, P. Ferrando, L. J. Haasbroek, H. Kunow, R. Müller-Mellin, C. Paizis, M. S. Potgieter, A. Raviart and G. Wibberenz, Spatial variation of >40 MeV/n nuclei fluxes observed during the Ulysses rapid latitude scan, *Astron. Astrophys., 316*, 538-546, 1996.

Hundhausen, A. J., Sizes and locations of coronal mass ejections: SMM observations from 1980 and 1984-1989, *J. Geophys. Res., 98*, 13,177-13,200, 1993.

Jokipii, J. R., Effects of three-dimensional heliospheric structures on cosmic-ray modulation, in *The Sun and the Heliosphere in Three Dimensions,* edited by R. G. Marsden, pp 375-387, D. Reidel, Dordrecht, 1986.

Jokipii, J. R. and J. Kota, The polar heliospheric magnetic field, *Geophys. Res. Lett., 16*, 1-4, 1989.

Jokipii, J. R., E. H. Levy and W. B. Hubbard, Effects of drift on the transport of cosmic rays, I. General properties, application to solar modulation, *Astrophys. J., 213*, 861, 1977.

Ko, Y.-K., L. A. Fisk, J. Geiss, G. Gloeckler and M. Guhathakurta, An empirical study of the electron temperature and heavy ion velocities in the south polar coronal hole, *Solar Phys., 171*, 345-361, 1997.

Kohl, J. L., et al., First results from the SOHO ultraviolet coronagraph spectrometer, *Solar Phys.*, 613-644,1997.

Lallement, R., R. E. Holzer and R. H. Munro, Solar wind expansion in a polar coronal hole: Inferences from coronal white light and interplanetary Lyman alpha observations, *J. Geophys. Res., 91*, 6751-6759, 1986.

Marubashi, K., Interplanetary magnetic flux ropes and solar filaments, in *Coronal Mass Ejections, Geophysical Monograph 99,* edited by N. Crooker, J. A. Joselyn and J. Feynman, pp 147-156, Amer. Geophys. Un., Washington, DC, 1997.

McComas, D. J., B. L. Barraclough, J. T. Gosling, C. M. Hammond, M. Neugebauer, A. Balogh and R. Forsyth, Structures in the polar solar wind: plasma and field observations from Ulysses, *J. Geophys. Res., 100*, 19,893-19,902, 1995.

McComas, D. J., G. W. Hoogeveen, J. T. Gosling, J. L. Phillips, M. Neugebauer, A. Balogh and R. Forsyth, Ulysses observations of pressure-balance structures in the polar solar wind, *Astron. Astrophys., 316*, 368-373, 1996.

McComas, D. J., et al., Ulysses' return to the slow solar wind, *Geophys. Res. Lett., 25*, 1, 1998.

McKenzie, J. F., B. Banaszkiewicz and W. I. Axford, Acceleration of the high speed solar wind, *Aston. Astrophys., 303*, L45-L48, 1995.

Neugebauer, M., B. E. Goldstein, D. J. McComas, S. T. Suess and A. Balogh, Ulysses observations of microstreams in the solar wind from coronal holes, *J. Geophys. Res., 100*, 23389, 1995.

Neugebauer, M., et al., The spatial structure of the solar wind and comparisons with solar data and models, *J. Geophys. Res., 103*, in press, 1998.

Nolte, J. T., A. S. Krieger, A. F. Timothy, R. E. Gold, E. C. Roelof, G. Vaiana, A. J. Lazarus, J. D. Sullivan and P. S. McIntosh, Coronal holes as sources of solar wind, *Solar Phys., 46*, 303, 1976.

Parker, E. N., Dynamics of the interplanetary gas and magnetic fields, *Astrophys. J., 128*, 664, 1958.

Roberts, D. A. and M. L. Goldstein, Evidence for a high-latitude origin of lower latitude high-speed wind, *Geophys. Res. Lett., 25*, 595-598, 1998.

Simpson, J. A., et al., Cosmic ray and solar particle investigations over the south polar regions of the Sun, *Science, 268*, 1019, 1995.

Smith, C. W. and J. W. Bieber, Solar cycle variation of the interplanetary magnetic field spiral, *Astrophys. J., 370*, 435-441, 1991.

Smith, E. J., A. Balogh, M. Neugebauer and D. McComas, Ulysses observations of Alfvén waves in the southern and northern solar hemispheres, *Geophys. Res. Lett., 22*, 3381, 1995.

Smith, E. J., A. Balogh, M. E. Burton, R. Forsyth, and R. P. Lepping, Radial and azimuthal components of the heliospheric magnetic field: Ulysses observations, *Adv. Space Res., 20, No. 1*, 47, 1997.

Snodgrass, H. B., Magnetic rotation of the solar photosphere, *Astrophys. J., 270*, 288, 1983.

Suess, S. T., Models of coronal hole flows, *Space Sci. Rev., 23*, 159, 1979.

Suess, S. T. and E. J. Smith, Latitudinal dependence of the radial IMF component: Coronal imprint, *Geophys. Res. Lett., 23*, 3267-3270, 1996.

Thieme, K. M., E. Marsch and R. Schwenn, Relationship between structures in the solar wind and their source regions in the corona, in *Proceedings of the Sixth International Solar Wind Conference, NCAR/TN-306+Proc,* edited by V. J. Pizzo, T. E. Holzer and D. G. Sime, pp 317, National Center for Atmospheric Research, Boulder, CO, 1988.

Thieme, K. M., E. Marsch and R. Schwenn, Spatial structures in high-speed streams as signatures of fine structures in coronal holes, *Ann. Geophys., 8*, 713, 1990.

Thomson, D. J., C. G. Maclennan and L. J. Lanzerotti, Evidence for solar g-mode modulation of interplanetary charged-particles and magnetic fields, *Nature, 376*, 139, 1995.

Wang, Y.-M. and N. R. Sheeley, Jr., Why fast solar wind originates from slowly expanding coronal flux tubes, *Astrophys. J., 372*, L45, 1991.

Wang, Y.-M., N. R. Sheeley, Jr., J. L. Phillips and B. E. Goldstein, Solar wind stream interactions and the wind speed-expansion factor relationship, *Astrophys. J., 488*, L51-L54, 1997.

Woo, R. and S. R. Habbal, Extension of coronal structure into interplanetary space, *Geophys. Res. Lett., 24*, 1159-1162, 1997.

Woo, R. and J. M. Martin, Source regions of the slow solar wind, *Geophys. Res. Lett., 24*, 2535, 1997.

Table 1. Comparison of coronal mass ejections observed in the solar wind at low and high latitudes

Feature	Low Latitude	High Latitude
Speed	Moderate, ~ Ambient	Fast, ~ Ambient
Shocks	Ahead of CME	Ahead of and behind CME
Bi-Directional Streaming?	Yes	Yes
Magnetic Clouds?	Some	Some
Ionization Temperature	> Ambient or Mixed	~ Ambient
Alpha Abundance	> Ambient	~ Ambient

Figure Captions

Figure 1. A polar plot of solar-wind speed versus heliographic latitude observed by Ulysses, with aphelion observations on the right and perihelion observations on the left. The speed is color coded according to the polarity of the interplanetary magnetic field, with fields pointing away from the Sun indicated by red and inward fields indicated by blue. Also included are snapshots of the Sun as viewed near solar minimum by the EIT instrument on SOHO (disk image), the Mauna Loa coronameter (low corona), and the LASCO instrument on SOHO (outer corona). Figure from *McComas et al.* [1998]

Figure 2. Plot of heliographic latitude versus distance from the Sun along the trajectory of the Ulysses spacecraft. Each point represents an average location over one solar rotation as seen from the vantage point of Ulysses.

Figure 3. Solar-rotation averages of solar wind speed as observed by the Ulysses spacecraft. Dashed and solid lines denote data taken in the southern and northern hemispheres, respectively.

Figure 4. Polar coronal electron temperature as calculated from coronagraph data on the assumption of hydrostatic equilibrium (+ symbols) and from the ionization charge state distribution of heavy ions in the polar solar wind (solid curve). Figure from *Ko et al.* [1997].

Figure 5. Superposed epoch plot showing variations associated with solar rotation. The parameters plotted are the alpha-particle speed V_α, the ionization temperature T_O calculated from the relative abundances of the O^{7+} and O^{6+} ions, and the ratio of the fluxes of Mg to O ions as observed by the SWICS instrument on Ulysses. Figure from *Geiss et al.* [1995].

Figure 6. Power spectra of the radial (R), tangential (T), and normal (N) components of the solar wind proton velocity during seven solar rotations when the Ulysses spacecraft was continuously in the high-speed flow from the south polar coronal hole. Figure from *Neugebauer et al.* [1995].

Figure 7. From top to bottom: solar wind speed, plasma pressure (nkT) and magnetic pressure ($B^2/8\pi$) for the period April 1-24, 1994, observed by Ulysses at a heliolatitude of ~60°S. Figure from *McComas et al.* [1995].

Figure 8. Superposed epoch analyses of variations of 6-hour averages of several plasma parameters with the zero epochs chosen at the maxima (left) or minima (right) of the speed fluctuations in the high-latitude solar wind observed in the southern hemisphere. From top to bottom are plotted the radial component of the proton velocity, the proton flux, normalized to 1 AU by the factor R^2; the proton temperature normalized to 1 AU by the factor $R^{0.51}$, and the ratio of alpha-particle to proton flux times 100. Figure from *Neugebauer et al.* [1995].

Figure 9. Ulysses observations of daily averages of the radial component B_R of the interplanetary magnetic field, normalized to a solar distance of 1 AU, versus time (bottom scale) and versus heliographic latitude (top scale). Figure from *Smith et al.* [1997].

Figure 10. (Heavy line) Value of the ratio of the radial component of the interplanetary magnetic field to the field magnitude expected for an ideal Parker spiral configuration. Each point represents a solar-rotation average of hourly averaged values $\langle B_R \rangle / \langle B \rangle$. (Dashed line) The observed values of the same ratio. (Thin line) The ratio expected for random fluctuations.

Figure 11. Histograms of the direction of the high-latitude interplanetary magnetic field (ϕ_B) relative to the expected Parker spiral angle (ϕ_P). Figure from *Forsyth et al.* [1996].

Figure 12. Correlation between the normal components of the proton velocity v_N and the magnetic field B_N along the Ulysses trajectory. Each point represents a solar rotation average calculated from hourly averages of v_N and B_N. The arrows indicate increasing time along the Ulysses trajectory (see Figure 2). As expected for Alfvén waves propagating away from the from Sun, the correlation is positive in the southern hemisphere where the interplanetary field is inward, and negative in the north where the field is outward.

Figure 13. A cartoon demonstrating the how the dragging of field lines by solar convection generates tangential fields at the solar polar surface. Figure from *Jokipii and Kota* [1989].

Figure 14. Projection of tracings of magnetic field lines originating at a latitude of 70°S according to (a) the Fisk model, and (b) the Parker spiral field. Figure from *Fisk* [1996].

Figure 15. Variation of the cosmic ray proton flux versus latitude in three different energy ranges for (a) a Parker-spiral field and (b) a modified spiral field as suggested by *Smith and Bieber* [1991], compared to the flux measured by the Ulysses KET instrument (dashed line in bottom panel). Figure from *Heber et al.* [1996].

Figure 16. (Top) Distribution of speeds of CMEs observed as they move through the inner coronal by the SMM spacecraft. (Bottom) Speeds of CMEs detected in situ by the plasma spectrometer on ISEE 3 (open circles) together with the speed distribution of all the solar wind detected by ISEE 3 (closed circles). The vertical lines in both panels indicate the

range of speeds of CMEs detected in the high-speed polar solar wind by Ulysses. Figure from *Gosling et al.* [1994a]

Figure 17. Some of the solar wind parameters observed during a CME event by IMP 8 near Earth (left) and by Ulysses at 3.53 AU and 54.3°S (right). From top to bottom are: the density, the proton temperature, the proton speed, the helium abundance relative to hydrogen, and the magnitude of the magnetic field. Figure from *Gosling* [1996].

Figure 18. A cartoon of a suggested geometry for a magnetic cloud. (The lines labeled A and B illustrate how the field rotation might appear for two different 1-dimensional cuts through the pattern, as would be observed by a spacecraft.) Figure from *Marubashi* [1997].

Figure 19. Oxygen ion charge states as observed in individual CME events by the SWICS instrument on Ulysses as a function of heliographic latitude. Figure from *Galvin* [1997].

Figure 20. Total electron column density between Earth and Ulysses plotted versus solar latitude (red line) superimposed on edge-enhanced images from the High Altitude Observatory MK III K-coronameter on Mauna Loa. The different images are for (a) day 59, (b) day 63, (c) day 67, and (d) day 68, all in 1995. Figure from *Woo and Habbal* [1997].

Figure 21. White light image of the corona taken with the LASCO C2 coronagraph on SOHO on January 17, 1997, on which have been superimposed a contour line corresponding to an O^{5+} ion outflow speed of ~94 km/s (white curve), the slit of the SOHO UVCS instrument from which the speeds were calculated (short, solid black lines), and extrapolations of ray structures back to the solar surface (long dashed black lines). The

yellow circle shows the size of the solar disk hidden behind the occulting disk of the coronagraph. Original figure from *Habbal et al.* [1997].

Figure 22. Dependence of the total Lyman-α intensity observed by the UVCS instrument on SOHO at a solar distance of 3 R_s. The angle θ is co-latitude. (Squares) Observations. (Solid line) An empirical model based on an assumption of latitudinal flow equatorwards from the polar regions. (Dashed line) An empirical model based on an assumption of radial flow. Figure from *Cranmer et al.* [1998].

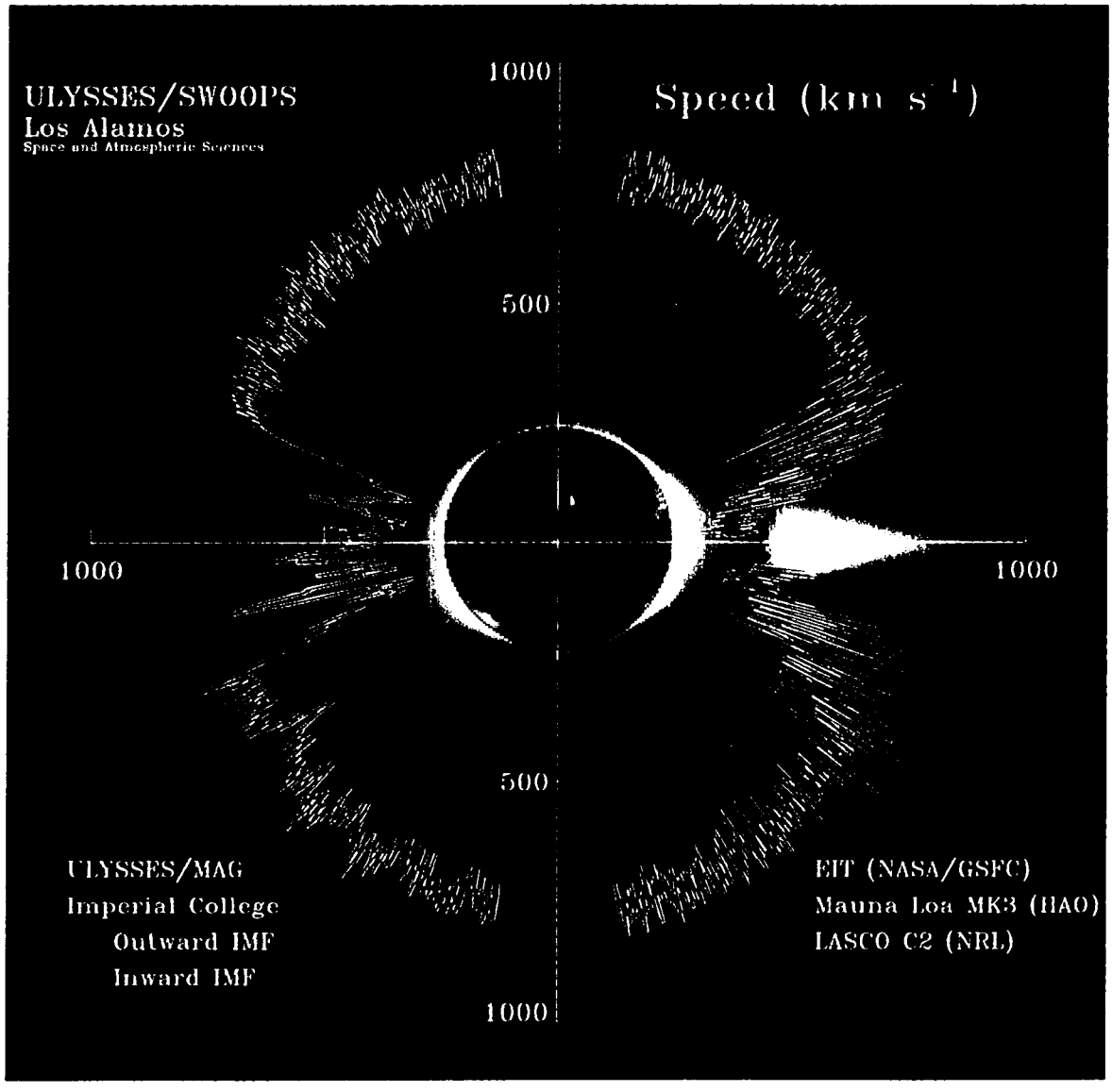
ULYSSES/SWOOPS
Los Alamos
Space and Atmospheric Sciences
Speed (km s⁻¹)
1000
500
1000
1000
500
1000
ULYSSES/MAG
Imperial College
Outward IMF
Inward IMF
EIT (NASA/GSFC)
Mauna Loa MK3 (HAO)
LASCO C2 (NRL)

Fig 1

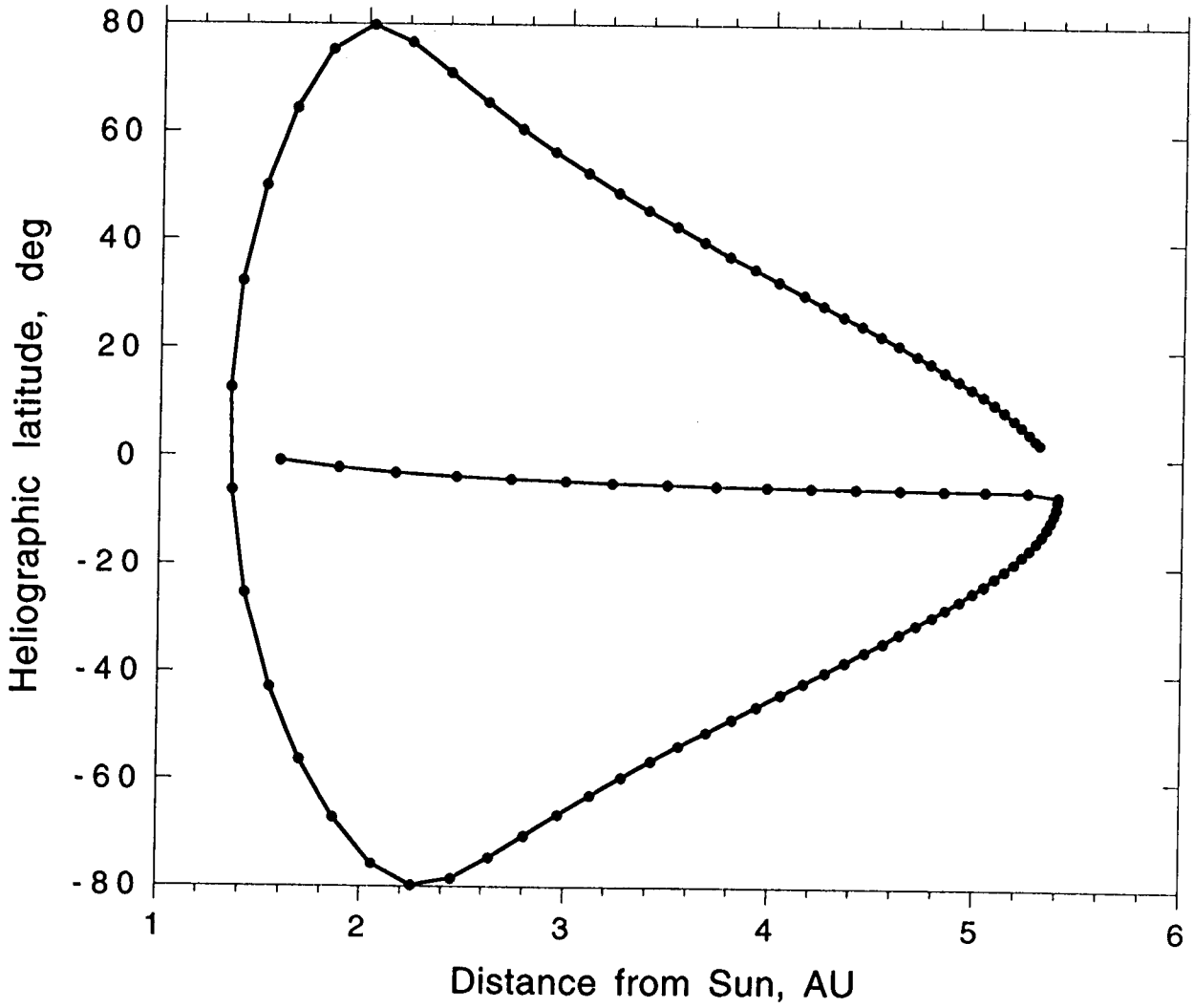
80
60
40
20
0
-20
-40
-60
-80
Heliographic latitude, deg
1
2
3
4
5
6
Distance from Sun, AU

Fig 2

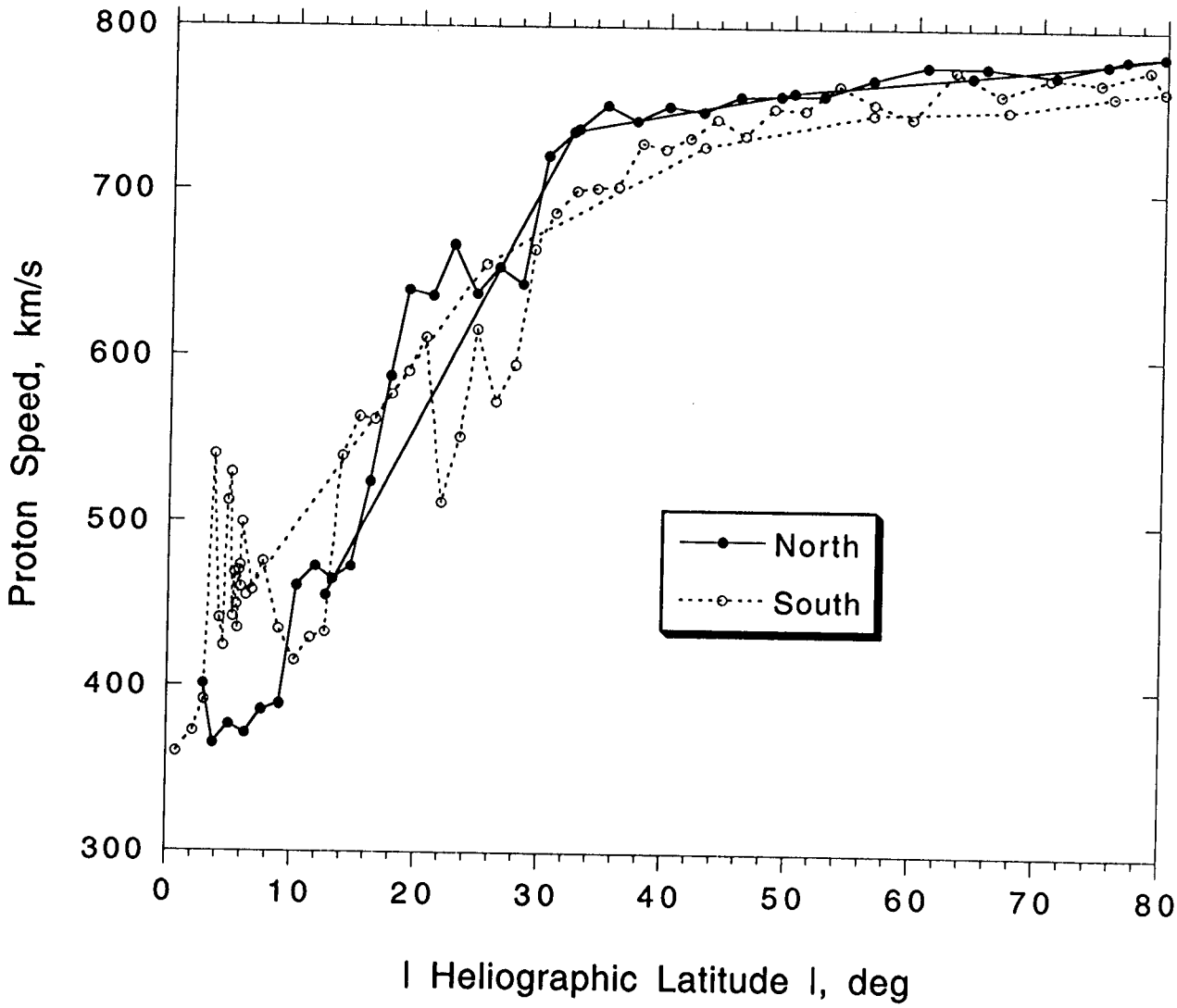
800
700
600
500
400
300
0
10
20
30
40
50
60
70
80
Proton Speed, km/s
| Heliographic Latitude |, deg
North
South

Fig 3

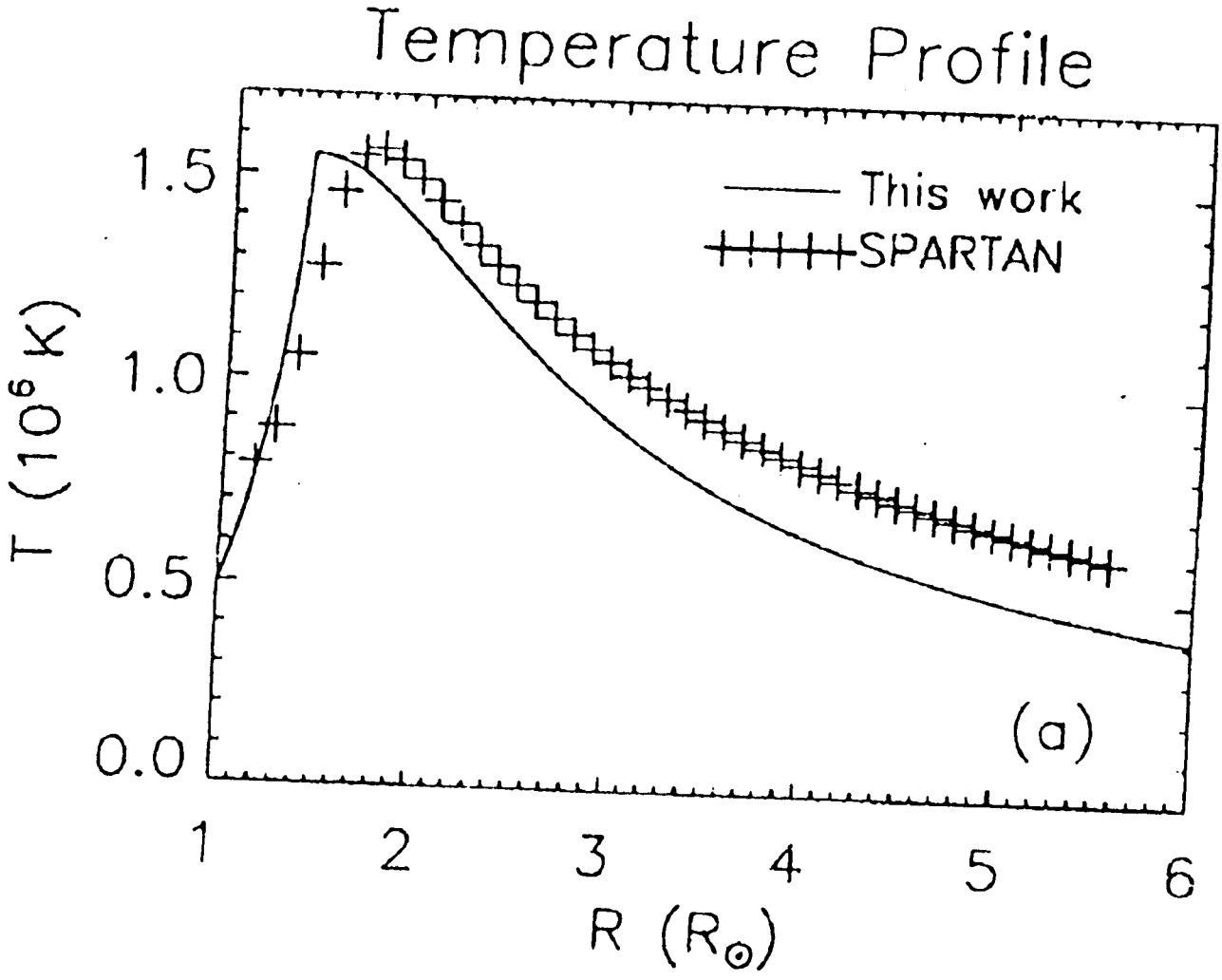
Temperature Profile
This work
SPARTAN
(a)
T (10^6 K)
1.5
1.0
0.5
0.0
1
2
3
4
5
6
R ($R_\odot$)

Fig 4

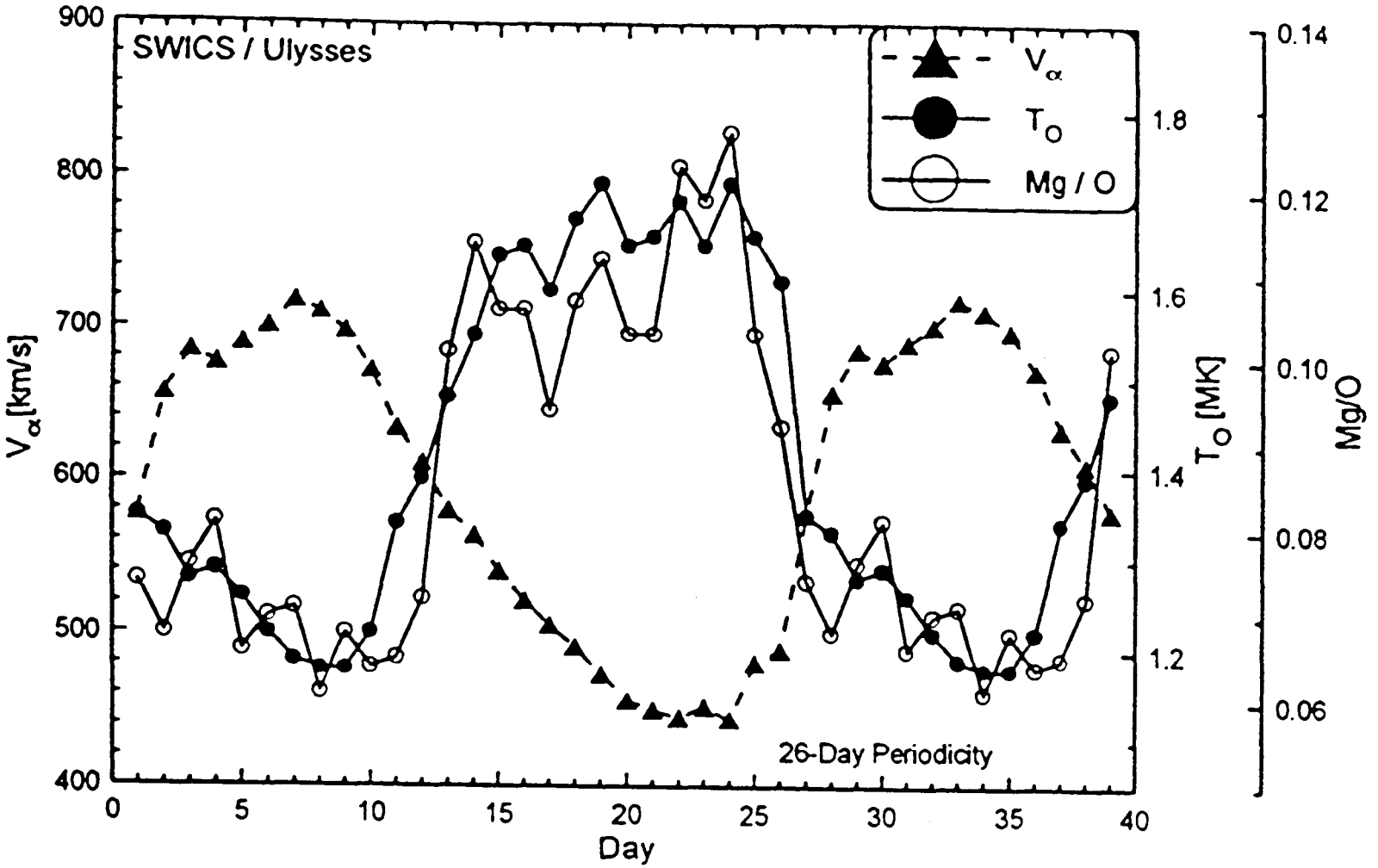
SWICS / Ulysses
V_α
T_O
Mg / O
26-Day Periodicity
V_α[km/s]
T_O [MK]
Mg/O
Day
900
800
700
600
500
400
1.8
1.6
1.4
1.2
0.14
0.12
0.10
0.08
0.06
0
5
10
15
20
25
30
35
40

Fig 5

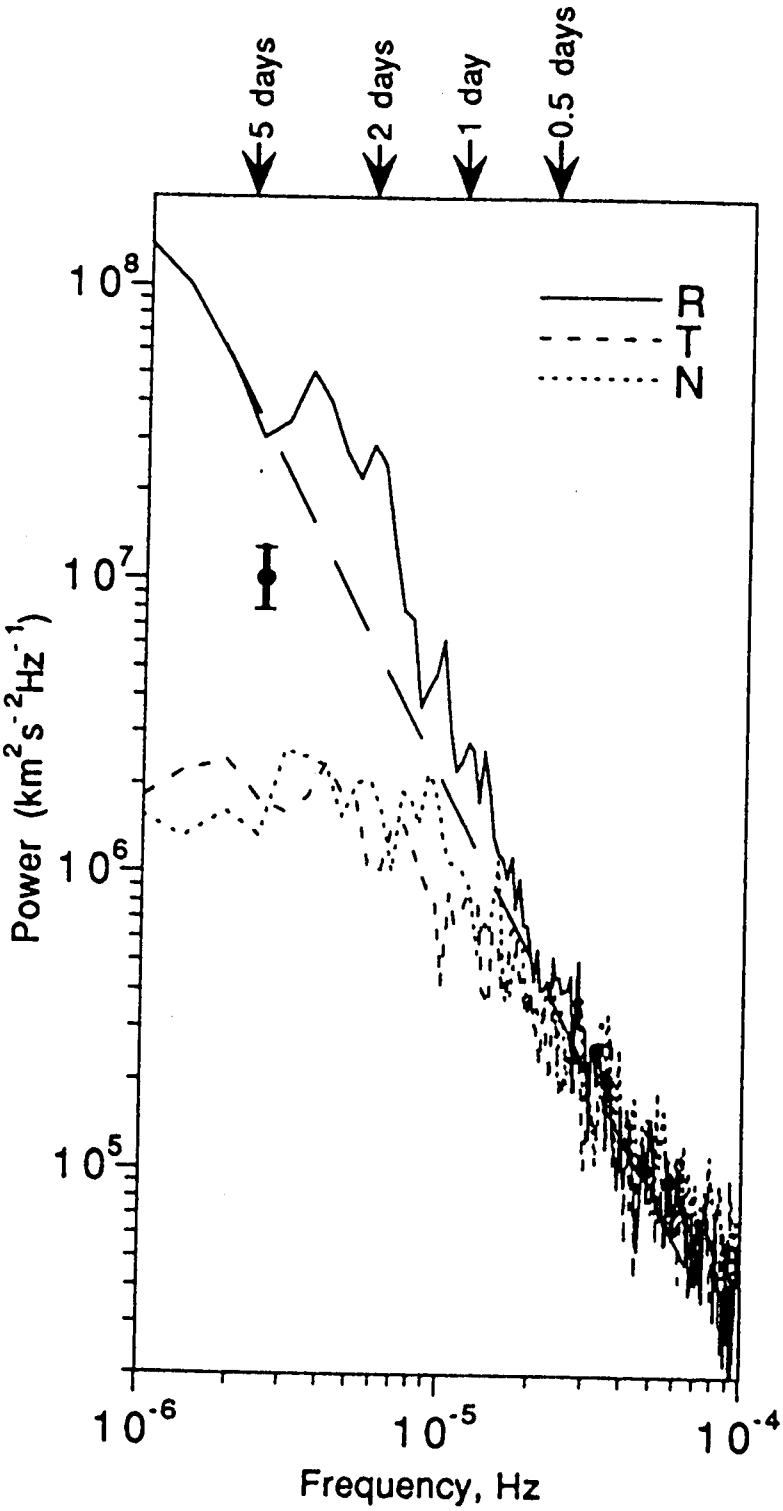
5 days
2 days
1 day
0.5 days
R
T
N
Power (km^{2}s^{-2}Hz^{-1})
10^8
10^7
10^6
10^5
10^{-6}
10^{-5}
10^{-4}
Frequency, Hz

Fig 6

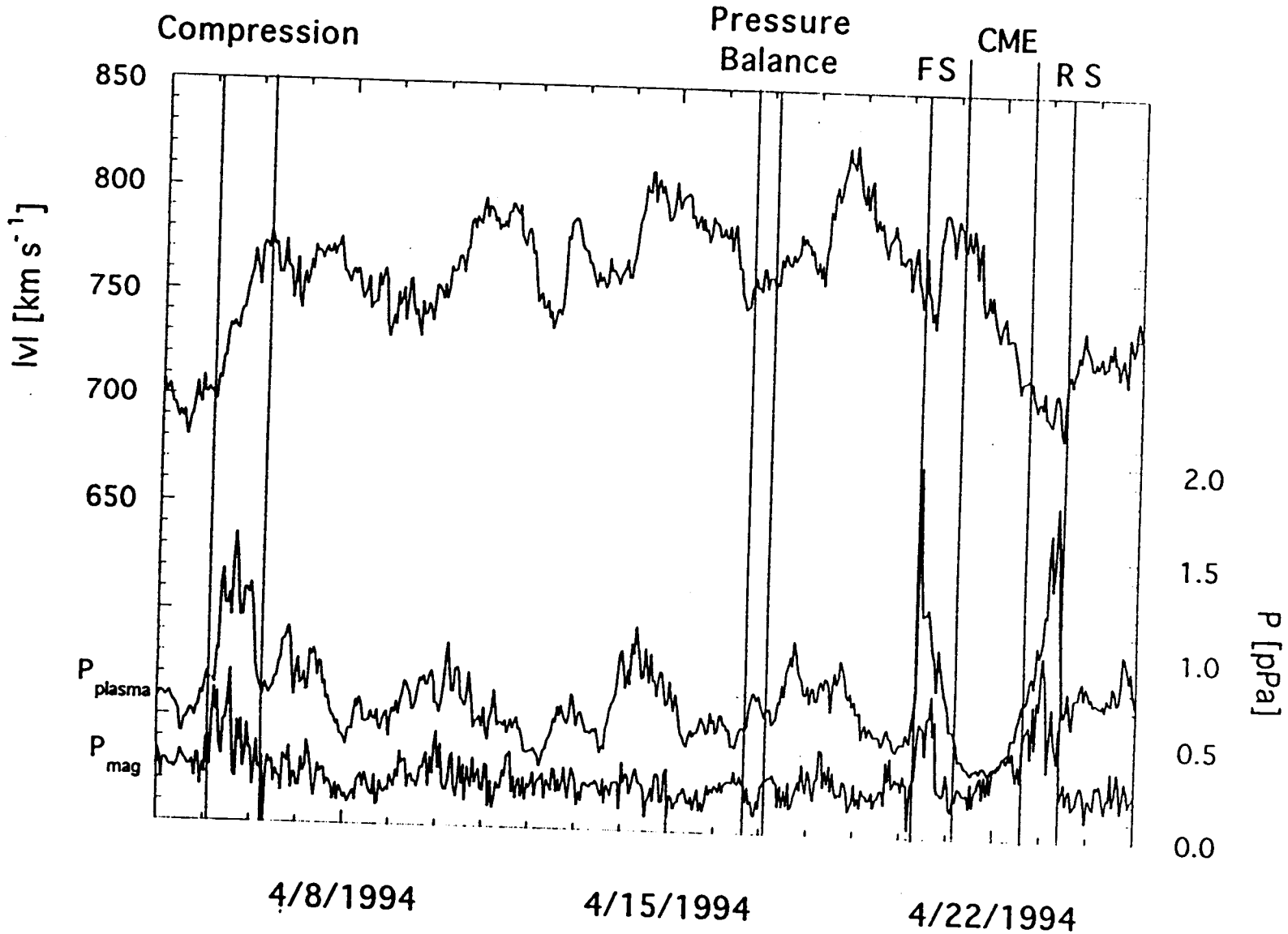
Compression
Pressure Balance
CME
FS
R S
850
800
750
700
650
|v| [km s^{-1}]
P_{plasma}
P_{mag}
2.0
1.5
1.0
0.5
0.0
P [pPa]
4/8/1994
4/15/1994
4/22/1994

Fig 7

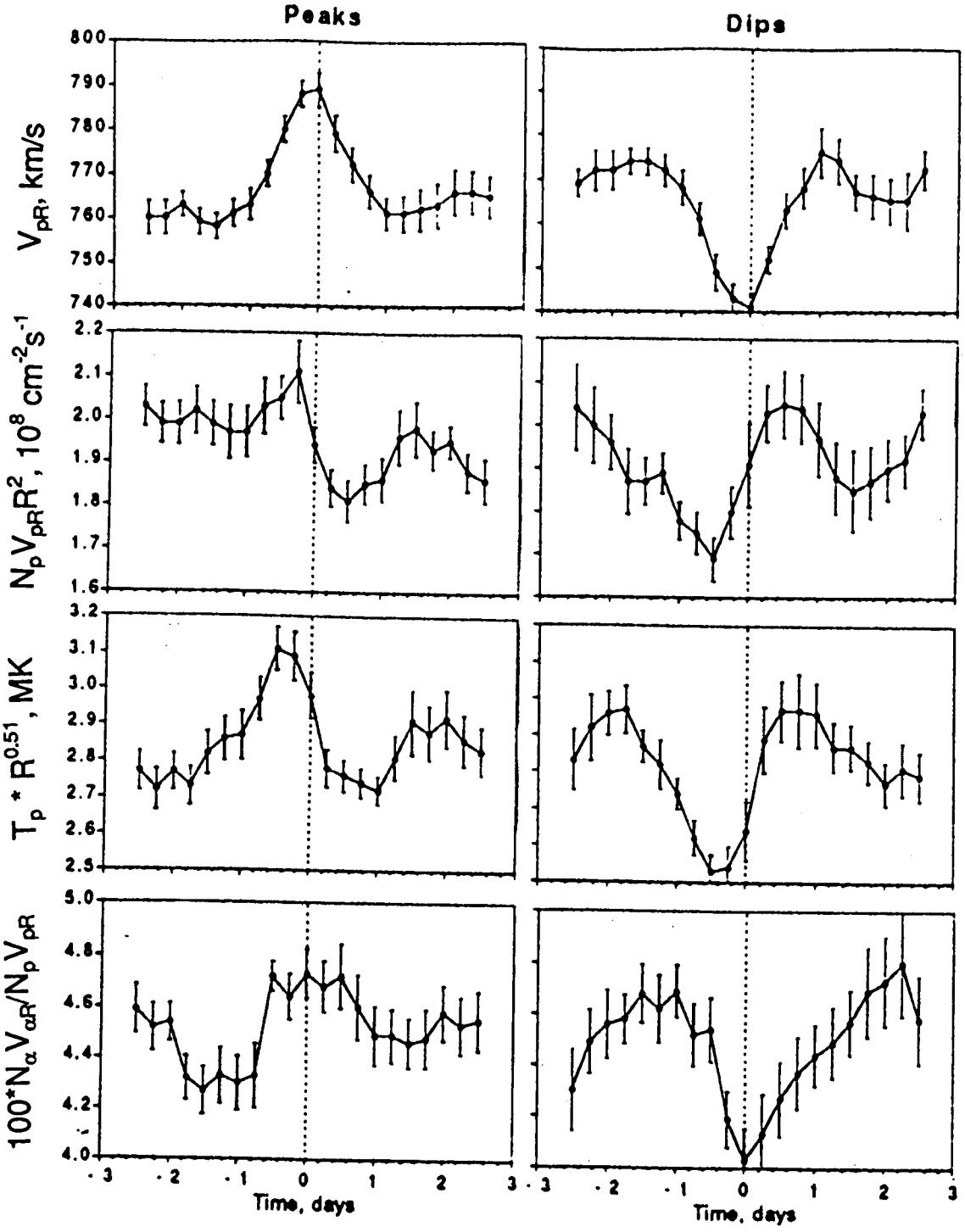
Peaks
Dips
V_{pR}, km/s
$N_p V_{pR} R^2$, 10^8 cm^{-2}s^{-1}
$T_p * R^{0.51}$, MK
$100*N_\alpha V_{\alpha R}/N_p V_{pR}$
Time, days
Time, days

Fig 8

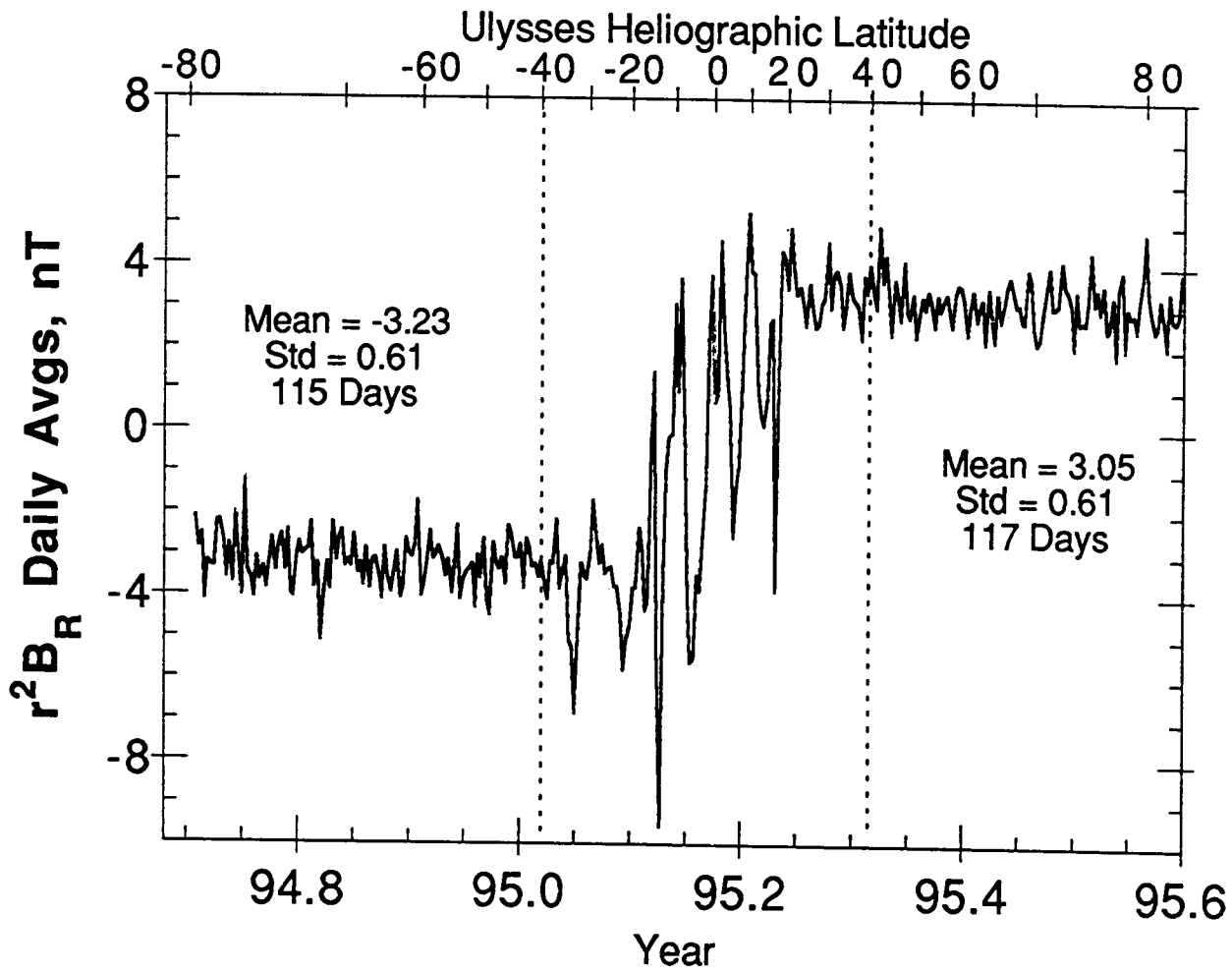
Ulysses Heliographic Latitude
-80
-60
-40
-20
0
20
40
60
80
8
4
0
-4
-8
r^2B_R Daily Avgs, nT
Mean = -3.23
Std = 0.61
115 Days
Mean = 3.05
Std = 0.61
117 Days
94.8
95.0
95.2
95.4
95.6
Year

Fig 9

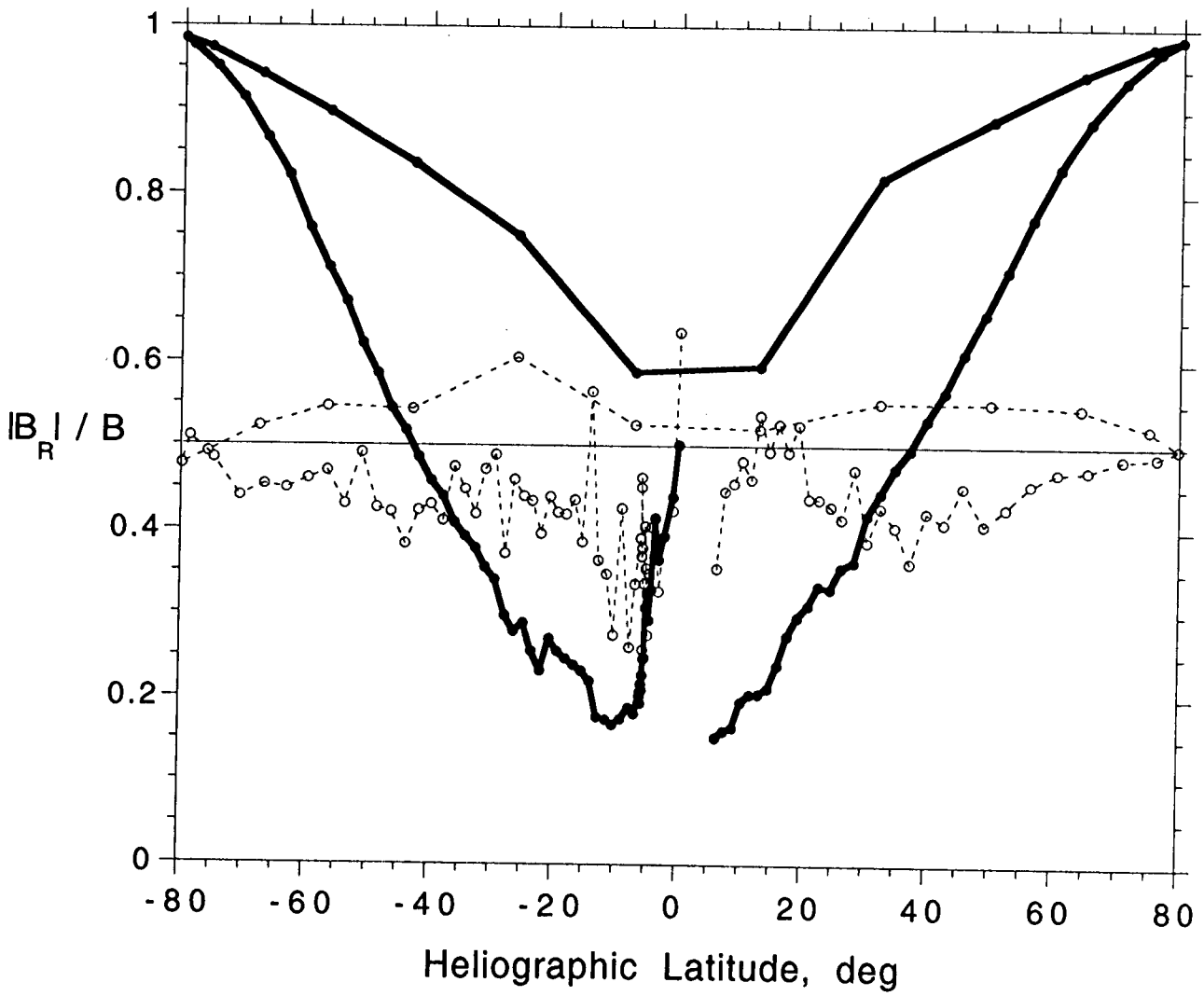
1
0.8
0.6
0.4
0.2
0
|B_R| / B
-80
-60
-40
-20
0
20
40
60
80
Heliographic Latitude, deg

Fig 10

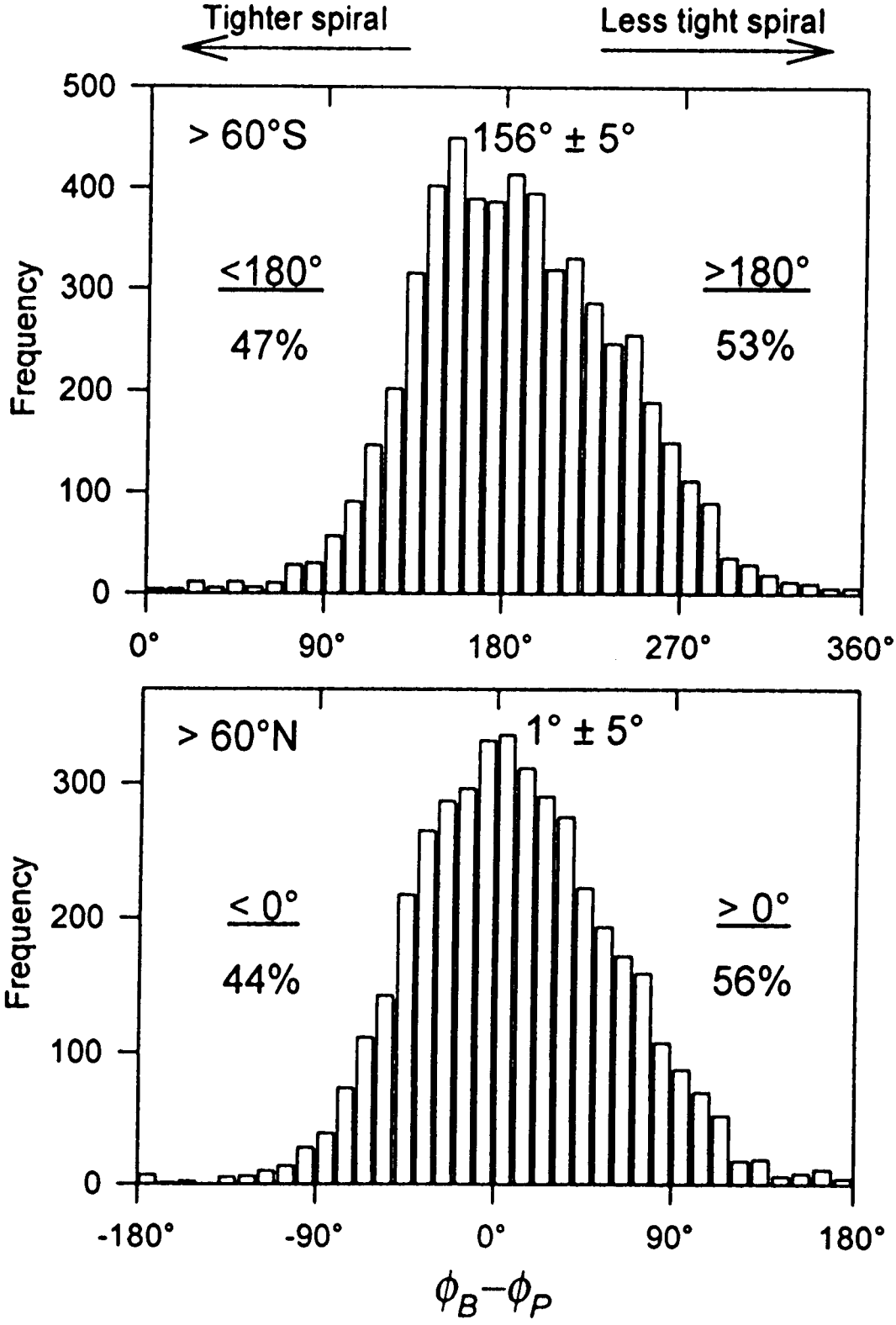
Tighter spiral
Less tight spiral
> 60°S
156° ± 5°
≤180°
47%
>180°
53%
Frequency
500
400
300
200
100
0
0°
90°
180°
270°
360°
> 60°N
1° ± 5°
≤ 0°
44%
> 0°
56%
Frequency
300
200
100
0
-180°
-90°
0°
90°
180°
$\phi_B - \phi_P$

Fig 11

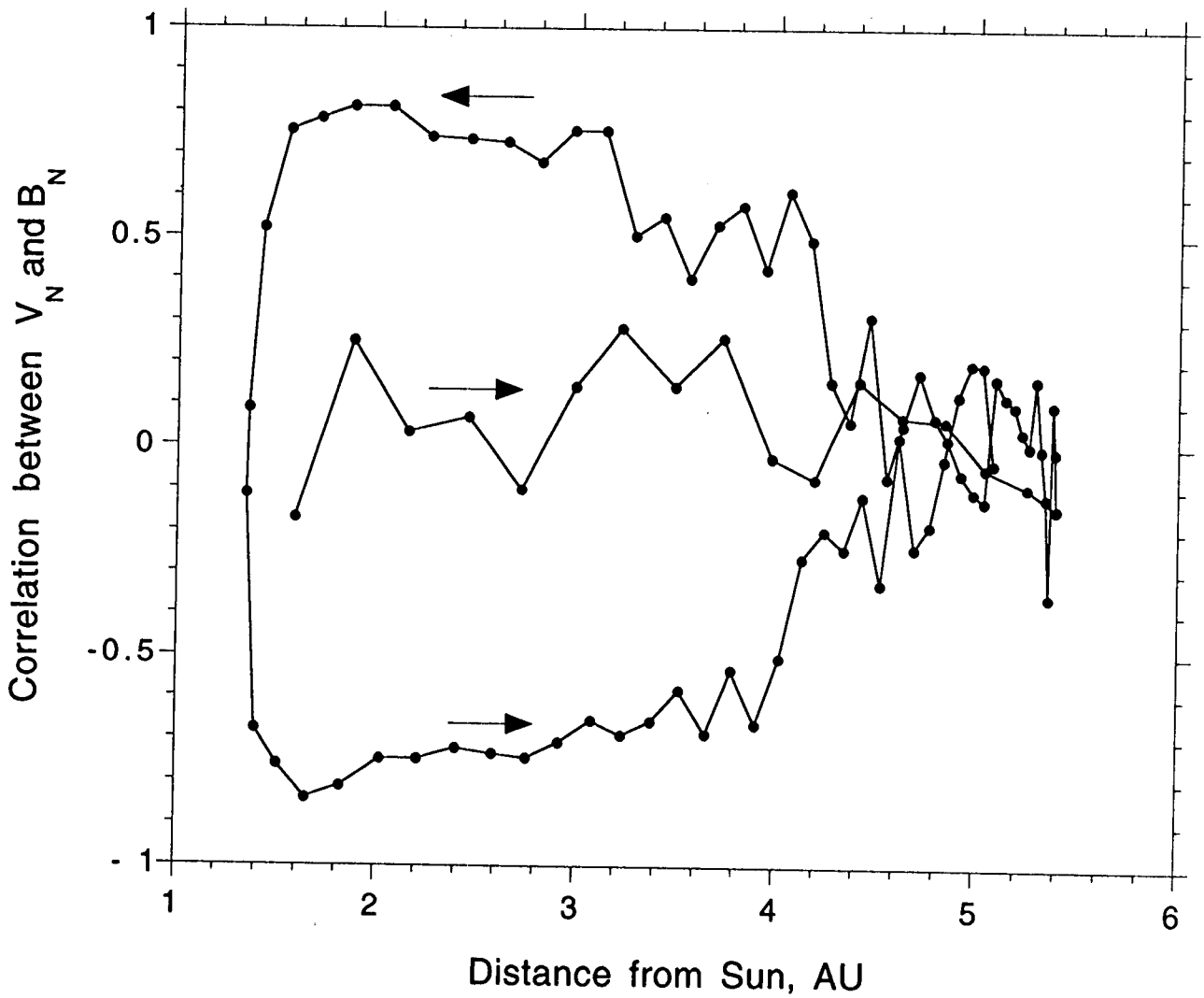
Correlation between V_N and B_N
1
0.5
0
-0.5
- 1
1
2
3
4
5
6
Distance from Sun, AU

Fig 12

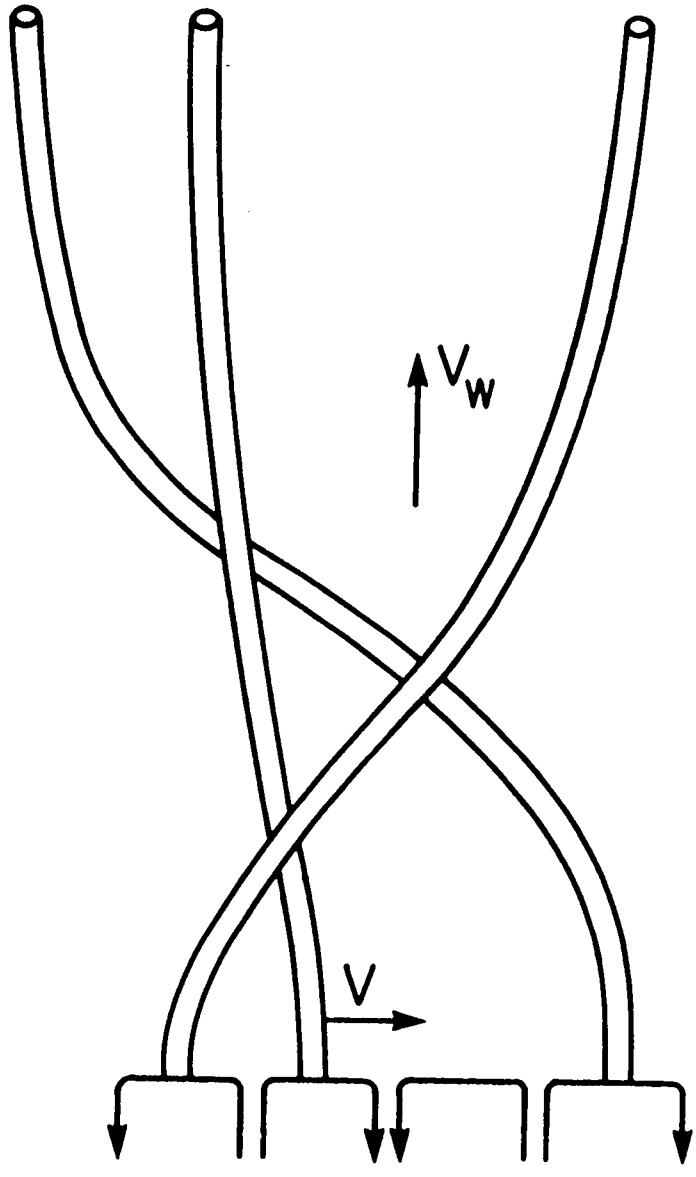

Fig 13

a

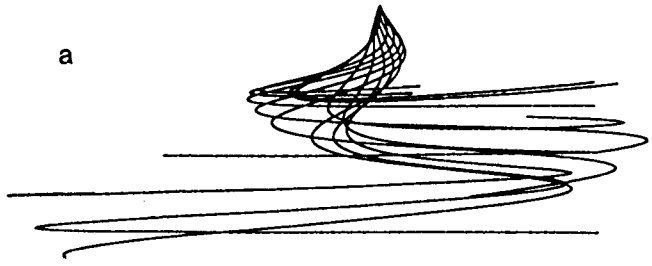

b

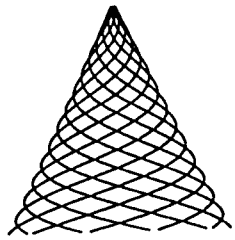

Fig 14

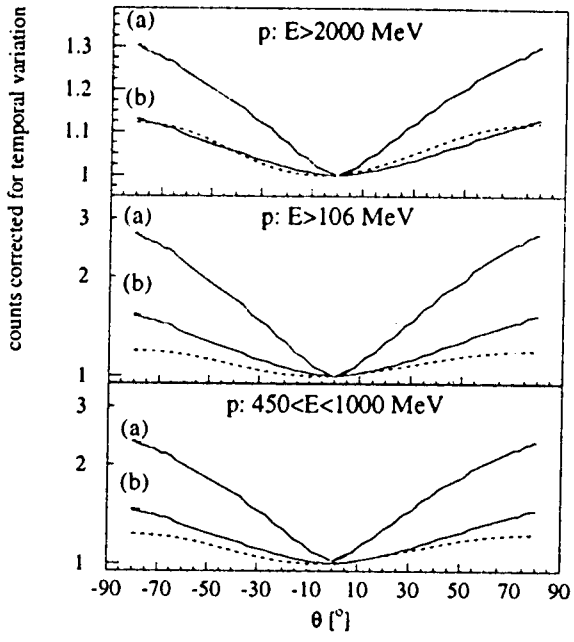
counts corrected for temporal variation
p: E>2000 MeV
(a)
(b)
1.3
1.2
1.1
1
p: E>106 MeV
(a)
(b)
3
2
1
p: 450<E<1000 MeV
(a)
(b)
3
2
1
-90 -70 -50 -30 -10 10 30 50 70 90
θ [°]

Fig 15

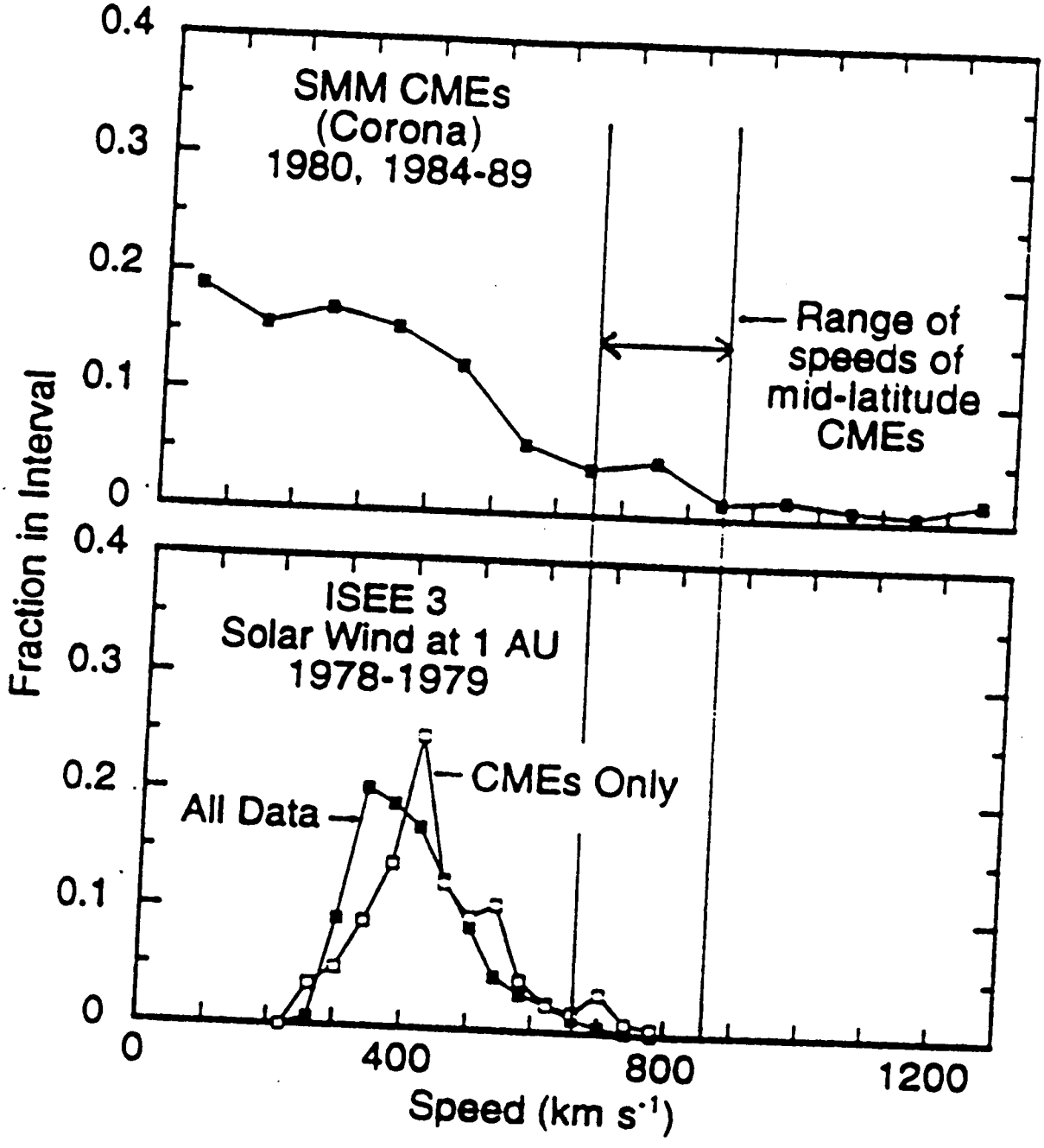
SMM CMEs
(Corona)
1980, 1984-89
Range of
speeds of
mid-latitude
CMEs
ISEE 3
Solar Wind at 1 AU
1978-1979
All Data
CMEs Only
Fraction in Interval
Speed (km s⁻¹)
0.4
0.3
0.2
0.1
0
400
800
1200

Fig 16

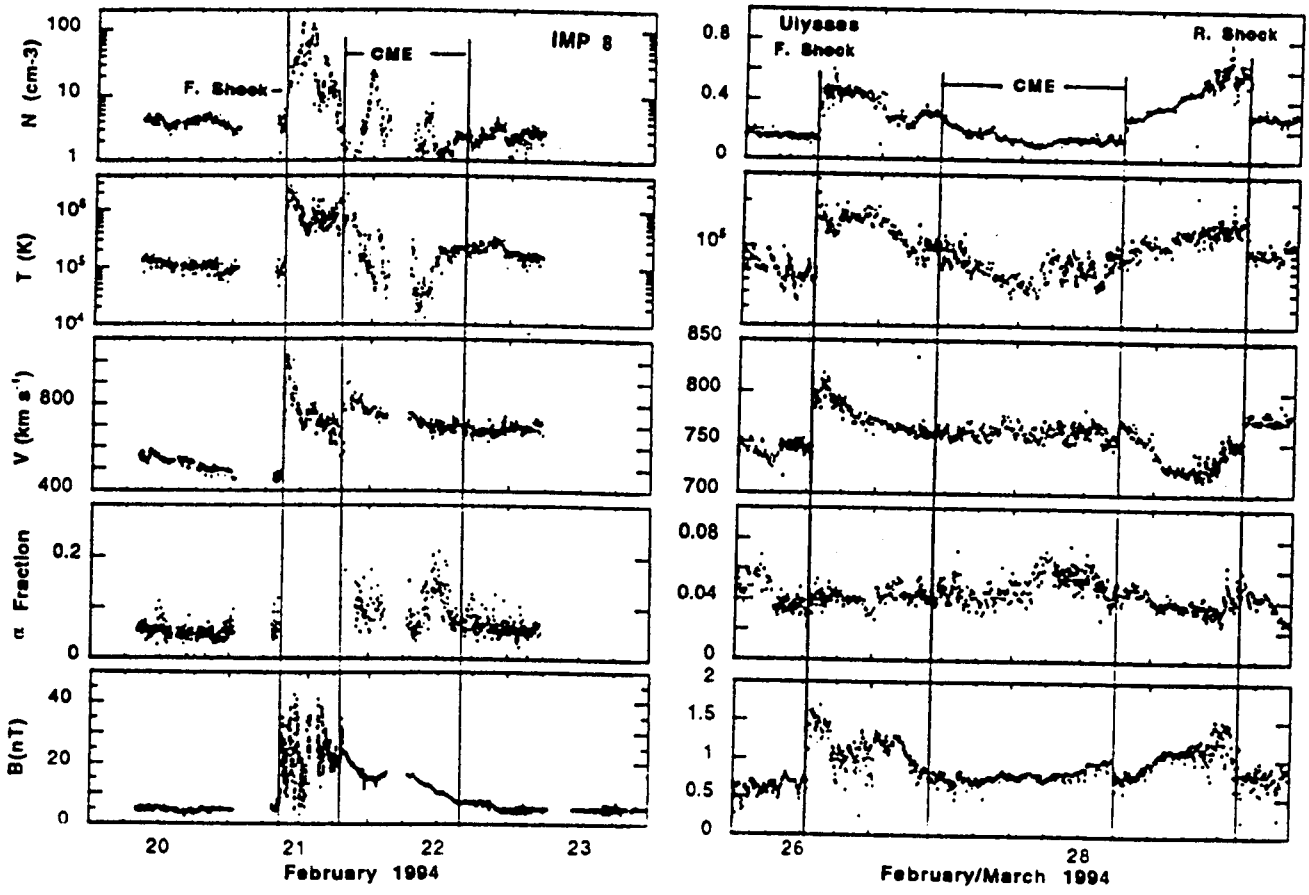
IMP 8
F. Shock
CME
N (cm-3)
T (K)
V (km s-1)
α Fraction
B(nT)
20
21
22
23
February 1994
Ulysses
F. Shock
R. Shock
CME
26
28
February/March 1994

Fig 17

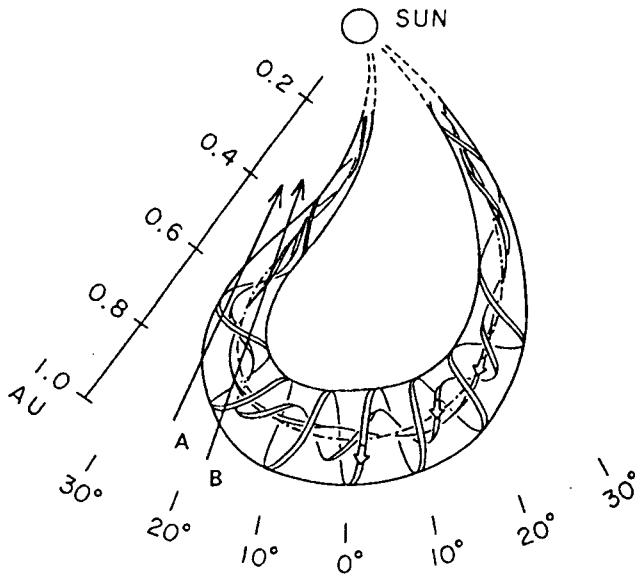

Fig 18

Ulysses SWICS CME-Related Solar Wind Oxygen Charge States Latitudinal Variations

(8° - 60° South HGLat)

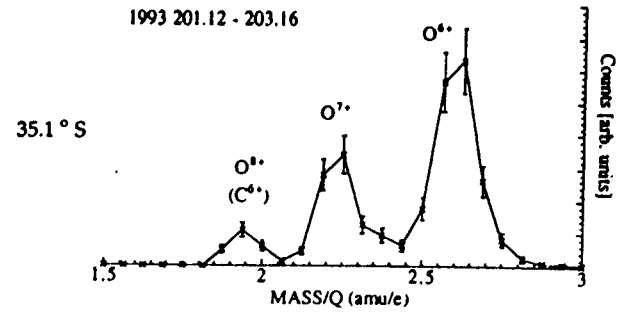

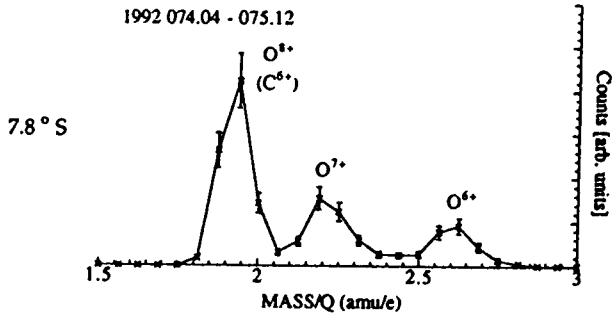

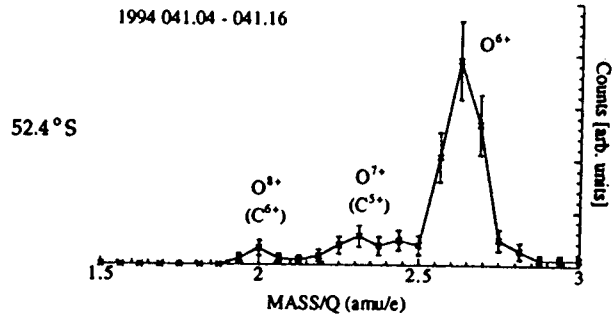

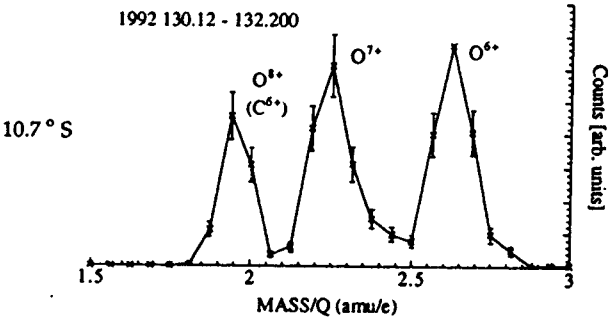

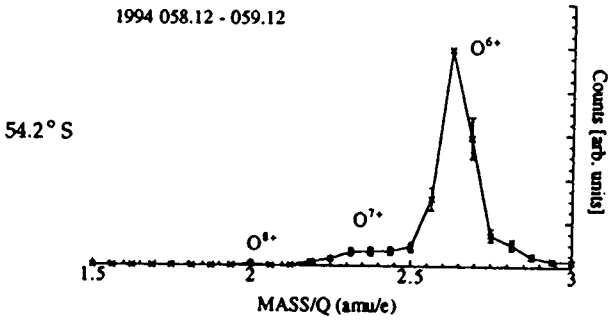

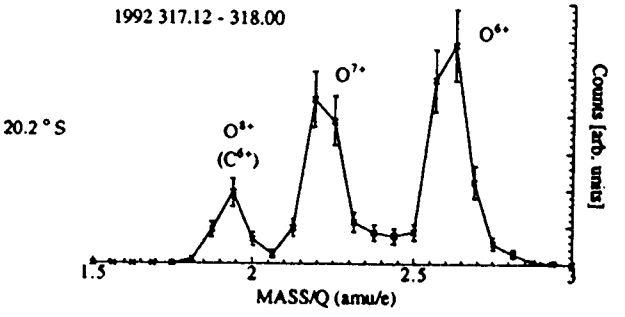

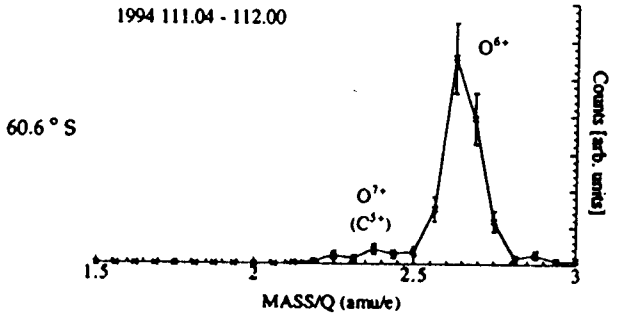

Fig. 19

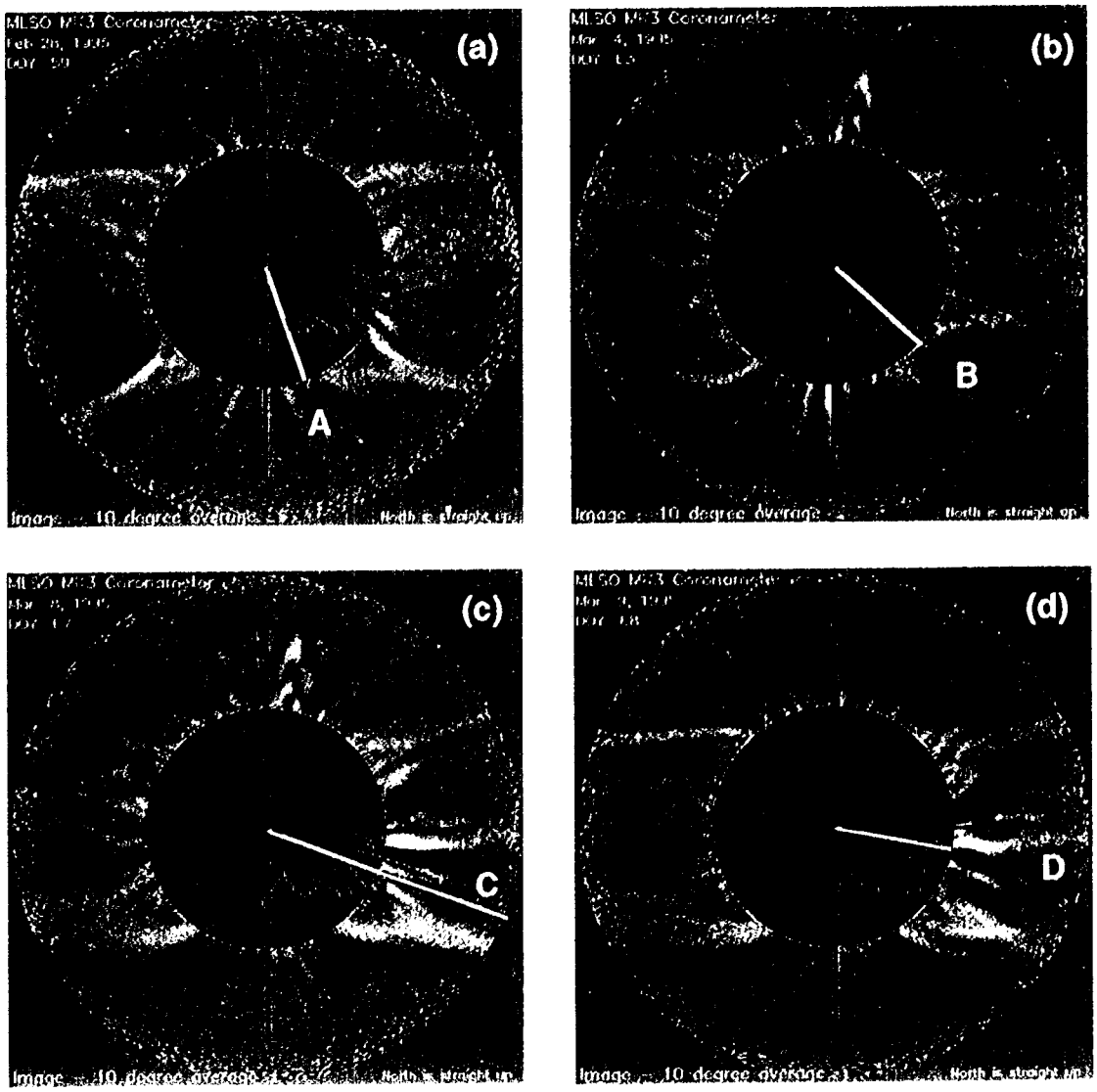

Fig 20

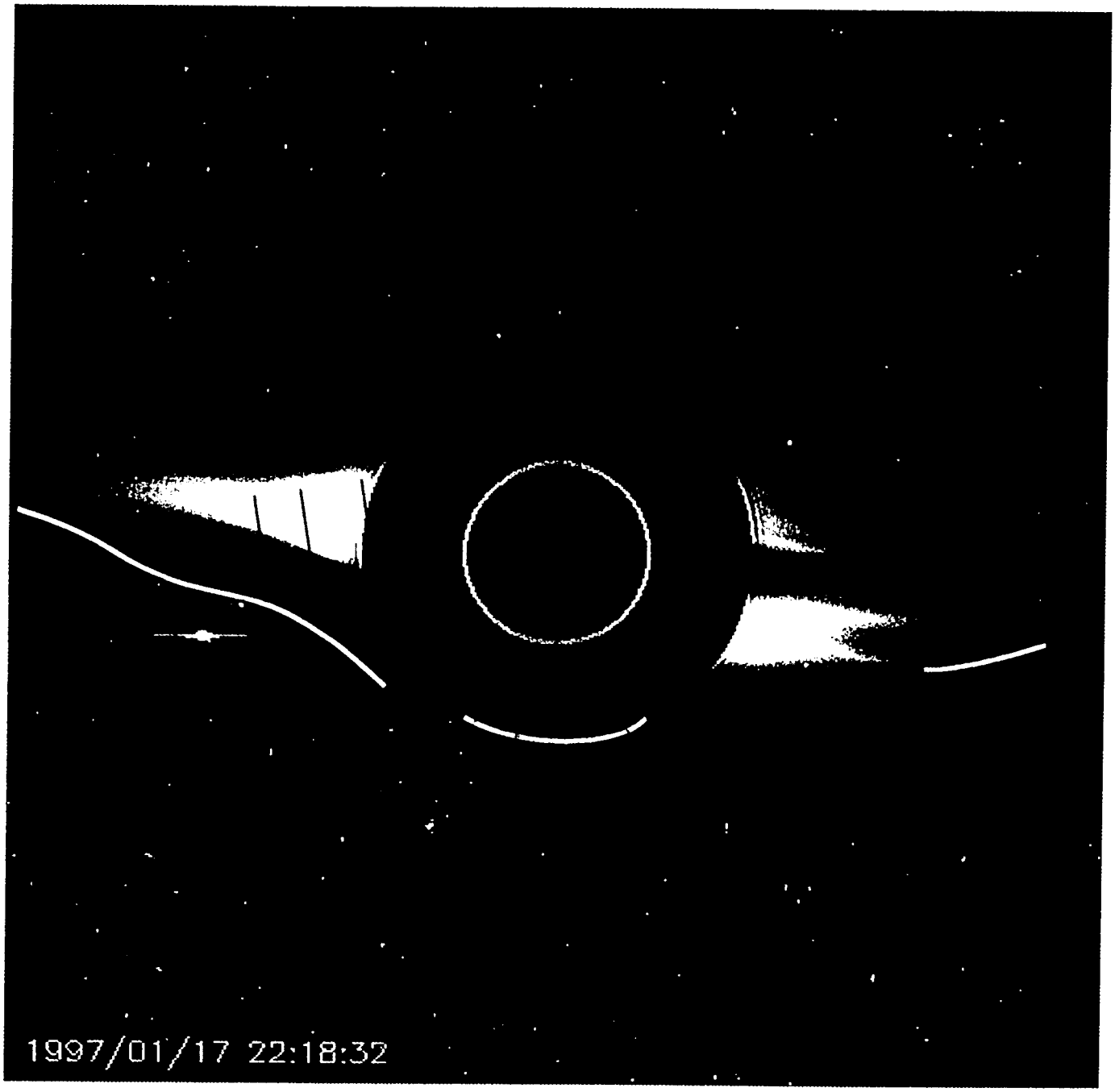

Fig 21

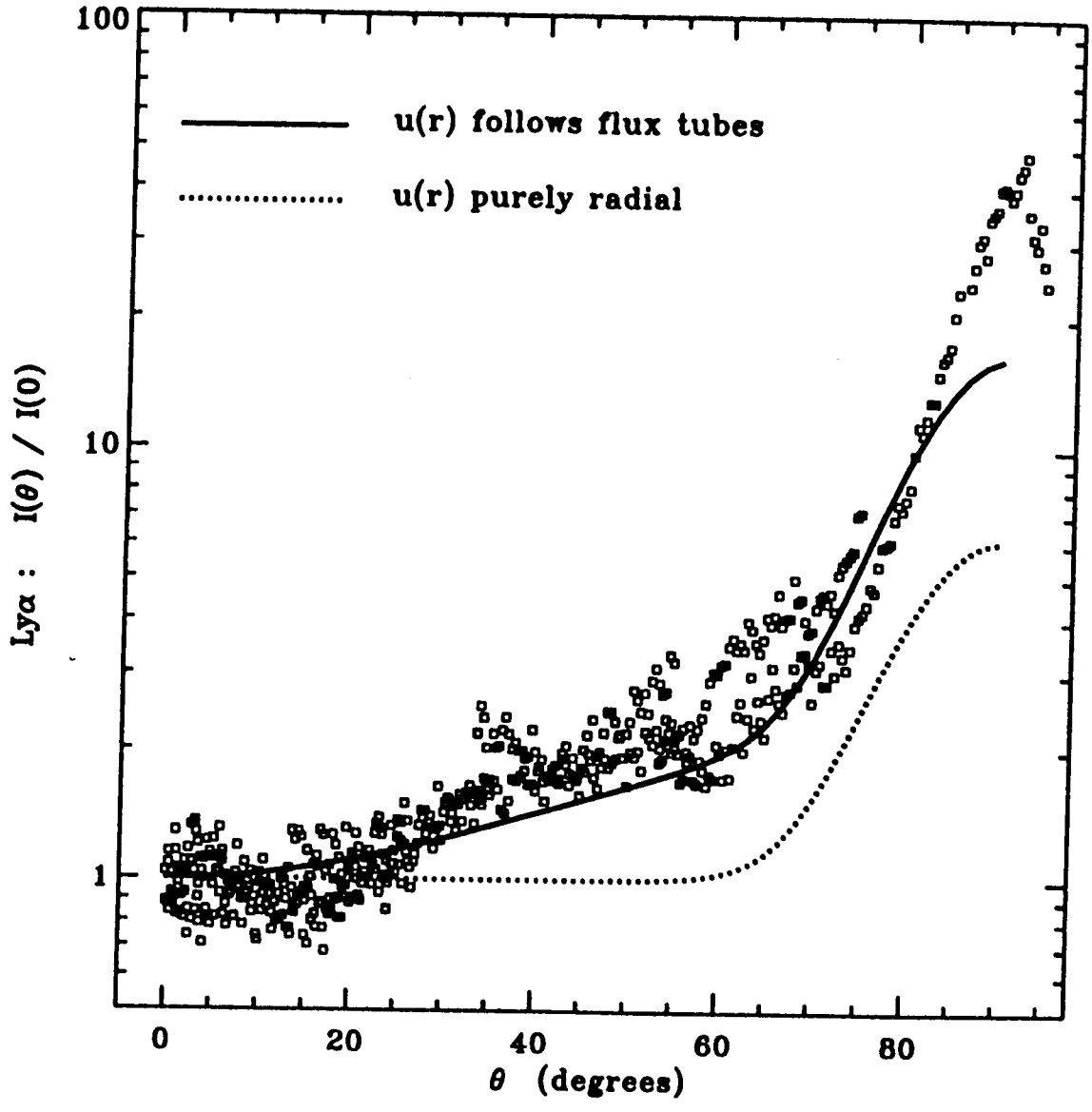
100
10
1
Lyα : I(θ) / I(0)
u(r) follows flux tubes
u(r) purely radial
0
20
40
60
80
θ (degrees)

Fig 22